



**HAL**  
open science

## Implications of the N-terminal heterogeneity for the neuronal K-Cl cotransporter KCC2 function

Marika Markkanen, Anastasia Ludwig, Stanislav Khirug, Evgeny Pryazhnikov, Shetal Soni, Leonard K Khiroug, Eric Delpire, Claudio Rivera, Matti S Airaksinen, Pavel Uvarov

► **To cite this version:**

Marika Markkanen, Anastasia Ludwig, Stanislav Khirug, Evgeny Pryazhnikov, Shetal Soni, et al.. Implications of the N-terminal heterogeneity for the neuronal K-Cl cotransporter KCC2 function. Brain Research, 2017, 1675, pp.87-101. 10.1016/j.brainres.2017.08.034 . hal-01961845

**HAL Id: hal-01961845**

**<https://hal.science/hal-01961845>**

Submitted on 20 Dec 2018

**HAL** is a multi-disciplinary open access archive for the deposit and dissemination of scientific research documents, whether they are published or not. The documents may come from teaching and research institutions in France or abroad, or from public or private research centers.

L'archive ouverte pluridisciplinaire **HAL**, est destinée au dépôt et à la diffusion de documents scientifiques de niveau recherche, publiés ou non, émanant des établissements d'enseignement et de recherche français ou étrangers, des laboratoires publics ou privés.

# Accepted Manuscript

Research report

Implications of the N-Terminal Heterogeneity for the Neuronal K-Cl cotransporter KCC2 Function

Marika Markkanen, Anastasia Ludwig, Stanislav Khirug, Evgeny Pryazhnikov, Shetal Soni, Leonard Khiroug, Eric Delpire, Claudio Rivera, Matti S. Airaksinen, Pavel Uvarov

PII: S0006-8993(17)30378-5

DOI: <http://dx.doi.org/10.1016/j.brainres.2017.08.034>

Reference: BRES 45476

To appear in: *Brain Research*

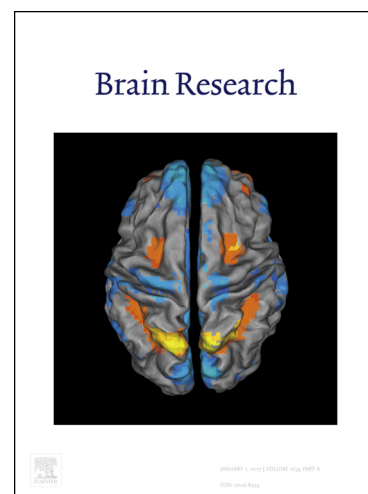
Received Date: 2 February 2017

Revised Date: 25 August 2017

Accepted Date: 30 August 2017

Please cite this article as: M. Markkanen, A. Ludwig, S. Khirug, E. Pryazhnikov, S. Soni, L. Khiroug, E. Delpire, C. Rivera, M.S. Airaksinen, P. Uvarov, Implications of the N-Terminal Heterogeneity for the Neuronal K-Cl cotransporter KCC2 Function, *Brain Research* (2017), doi: <http://dx.doi.org/10.1016/j.brainres.2017.08.034>

This is a PDF file of an unedited manuscript that has been accepted for publication. As a service to our customers we are providing this early version of the manuscript. The manuscript will undergo copyediting, typesetting, and review of the resulting proof before it is published in its final form. Please note that during the production process errors may be discovered which could affect the content, and all legal disclaimers that apply to the journal pertain.



## Implications of the N-Terminal Heterogeneity for the Neuronal K-Cl cotransporter KCC2 Function

Marika Markkanen<sup>1</sup>, Anastasia Ludwig<sup>2, #</sup>, Stanislav Khirug<sup>2</sup>, Evgeny Pryazhnikov<sup>2</sup>, Shetal Soni<sup>2</sup>, Leonard Khiroug<sup>2</sup>, Eric Delpire<sup>3</sup>, Claudio Rivera<sup>2, 4, 5</sup>, Matti S. Airaksinen<sup>1, \*</sup>, and Pavel Uvarov<sup>1, &, \*</sup>

<sup>1</sup> Department of Anatomy, Faculty of Medicine, University of Helsinki, Helsinki, Finland

<sup>2</sup> Neuroscience Center, University of Helsinki, Helsinki, Finland

<sup>3</sup> Department of Anesthesiology, Vanderbilt University School of Medicine, Nashville, TN, USA

<sup>4</sup> INSERM, Institut de Neurobiologie de la Méditerranée (INMED), Marseille, France

<sup>5</sup> Aix-Marseille Université, UMR901, Marseille, France

<sup>#</sup> The present address is École Normale Supérieure, Institut de Biologie de l'ENS (IBENS) INSERM CNRS PSL Research University, Paris, France

<sup>&</sup> The present address is Department of Biosciences and Neuroscience Center, University of Helsinki, Helsinki, Finland.

\* To whom correspondence may be addressed.

E-mail: [pavel.uvarov@helsinki.fi](mailto:pavel.uvarov@helsinki.fi) or [matti.airaksinen@helsinki.fi](mailto:matti.airaksinen@helsinki.fi)

Number of words in the body text [9235]

Number of figures: 7; number of supplementary figures: 6

**Abstract**

The neuron-specific K-Cl cotransporter KCC2 maintains the low intracellular chloride concentration required for the fast hyperpolarizing responses of the inhibitory neurotransmitters  $\gamma$ -aminobutyric acid (GABA) and glycine. The two KCC2 isoforms, KCC2a and KCC2b differ by their N-termini as a result of alternative promoter usage. Whereas the role of KCC2b in mediating the chloride transport is unequivocal, the physiological role of KCC2a in neurons has remained obscure. We show that KCC2a isoform can decrease the intracellular chloride concentration in cultured neurons and attenuate calcium responses evoked by application of the GABA<sub>A</sub> receptor agonist muscimol. While the biotinylation assay detected both KCC2 isoforms at the cell surface of cultured neurons, KCC2a was not detected at the plasma membrane in immunostainings, suggesting that the N-terminal KCC2a epitope is masked. Confirming this hypothesis, KCC2a surface expression was detected by the C-terminal KCC2pan antibody but not by the N-terminal KCC2a antibody in KCC2b-deficient neurons. One possible cause for the epitope masking is the binding site of Ste20-related proline-alanine-rich kinase (SPAK) in the KCC2a N-terminus. SPAK, a known regulator of K-Cl cotransporters, was co-immunoprecipitated in a complex with KCC2a but not KCC2b isoform. Moreover, SPAK overexpression decreased the transport activity of KCC2a but not that of KCC2b, as revealed by rubidium flux assay in HEK293 cells. Thus, our data indicate that both KCC2 isoforms perform as chloride cotransporters in neuronal cells, while their N-terminal heterogeneity could play an important role in fine-tuning of the K-Cl transport activity.

**Keywords**

intracellular chloride, KCC2, GABA, inhibition, SPAK

**Abbreviations**

$\gamma$ -aminobutyric acid (GABA), Ste20-related proline-alanine-rich kinase (SPAK), hemagglutinin-tagged SPAK protein (HA-SPAK), oxidative stress responsive kinase (OSR1), dominant negative form of SPAK (DN-SPAK)

## 1. Introduction

The neuronal K-Cl cotransporter KCC2 plays a central role in maintaining the low intracellular chloride concentration required for the fast hyperpolarizing responses of the inhibitory neurotransmitters GABA and glycine in mature neurons (Kaila et al., 2014). Mutations in the human gene encoding KCC2 (*SLC12A5*) are associated with several epilepsy syndromes (Kahle et al., 2014; Puskarjov et al., 2014; Stodberg et al., 2015; Saitsu et al., 2016). KCC2 expression is strongly up-regulated during neuronal maturation that leads to the developmental shift in the responses of ionotropic GABA<sub>A</sub> and glycine receptors (GABA<sub>A</sub>R and GlyR) from depolarizing in immature neurons to hyperpolarizing in adult neurons (Rivera et al., 1999). Besides the chloride extrusion function, KCC2 is also known to promote formation and maintenance of dendritic spines by interacting with the dendritic cytoskeleton (Li et al., 2007; Llano et al., 2015).

KCC2 has two full-length isoforms, KCC2a and KCC2b, which differ only in their most N-termini as a result of the alternative promoter and first exon usage (Uvarov et al., 2007). KCC2b isoform accounts for about 90 % of the total KCC2 expression in the adult mouse, and about a half of total KCC2 protein in the neonatal mouse (Uvarov et al., 2009). Both isoforms are expressed in the developing and adult hypothalamus, brainstem, and spinal cord (Markkanen et al., 2014). KCC2b expression increases steeply during postnatal development and is widely distributed in the adult brain, while KCC2a expression remains low or absent in the adult cortex, hippocampus, thalamus, and cerebellum (Markkanen et al., 2014). In addition to the two full-length KCC2 isoforms, a number of alternatively spliced truncated KCC2 variants have been reported (Tao et al., 2012).

Previous studies suggested involvement of the N-terminus of the K-Cl cotransporters into regulation of the transport activity (Casula et al., 2001; Shen et al., 2003; Li et al., 2007; Horn et al., 2010; Fiumelli et al., 2013). The 40-amino-acid long N-terminus unique for KCC2a contains the binding motif for SPAK (Uvarov et al., 2007). This SPAK binding sequence RFX(V/I) is also present in N-terminal domains of other CCC family isoforms (Delpire and Gagnon, 2008; Richardson et al., 2008) and is evolutionary conserved, being found in N-termini of KCC2 orthologs in *Drosophila* (Hekmat-Scafe et al., 2006) and *C. elegans* (Tanis et al., 2009). During the last few years multiple studies have elucidated the important role of the WNK-SPAK signaling pathway in the regulation of KCC2 transport activity (Inoue et al., 2012; de Los Heros et al., 2014; Friedel et al., 2015) and for review (Kahle and Delpire, 2016). The WNK-SPAK signaling pathway was shown to efficiently inhibit the K-Cl cotransport activity, even though the KCC2b variant, which lacks the RFX(V/I) motif, was used in most of these studies. This raises the question whether the SPAK binding motif in KCC2a is dispensable for the KCC2 regulation by the WNK-SPAK pathway.

Another open question is whether KCC2a is able to mediate K-Cl cotransporter activity in mature neurons. While both KCC2 isoforms demonstrate similar levels of the chloride transport activity in HEK293 cells (Uvarov et al., 2007), this has not been demonstrated in neuronal cells. A functional importance of KCC2a seems evident since KCC2 null mice that lack both KCC2 isoforms die at birth (Hubner et al., 2001; Tornberg et al., 2005), while KCC2b-deficient mice, which retain KCC2a, survive up to three weeks postnatally (Woo et al., 2002). Yet, KCC2a-deficient mice survive to adulthood and do not reveal any obvious phenotype (Markkanen et al., 2014), suggesting that KCC2b can compensate for the lack of KCC2a. Moreover, although both KCC2 isoforms are expressed in neonatal spinal motoneurons (Uvarov et al., 2007; Uvarov et al., 2009; Markkanen et al., 2014), recordings from KCC2b-deficient mice demonstrated a more depolarized glycine reversal potential (Stil et al., 2011)

similar to that found in motoneurons of KCC2 null mice (Hubner et al., 2001). One explanation for that fact could be the relatively low expression of the KCC2a in the spinal cord: the KCC2a isoform contributes 20-50 % to the total KCC2 protein level during first postnatal week, decreasing to 20 % in adulthood (Uvarov et al., 2009; Stil et al., 2011). Another reason could be the attenuated transport activity of KCC2a in the spinal cord motoneurons as the result of kinetic regulation by protein kinases.

In the current study we attempted to resolve these contradictions. We determined that both KCC2 isoforms are present at the neuronal surface, and that the KCC2a isoform, similar to KCC2b, can perform as the functional K-Cl cotransporter to maintain the low intracellular chloride concentration in neurons. We also found that the N-terminal epitope of KCC2a but not KCC2b can be masked at the neuronal plasma membrane, possibly due to the interaction with SPAK kinase. The differential interaction of the KCC2a and KCC2b isoforms with SPAK might imply a more stringent control of the KCC2a isoform by the WNK-SPAK pathway.

## 2. Results

### 2.1 Proportion of KCC2a to total KCC2 protein and mRNA expression decreases gradually with maturation of dissociated cortical cultures

Previous analysis of dissociated cortical neurons derived from KCC2b-knockout embryos did not reveal any significant decrease in intracellular chloride concentration  $[Cl^-]_i$  after 3 weeks in culture in contrast to the significant decrease of  $[Cl^-]_i$  in wild-type neurons (Zhu, Lovinger, Delpire, 2005). Although that study confirmed the important role of KCC2b for chloride homeostasis in more mature cortical neurons, the relative contribution of KCC2a was not addressed.

To assess the proportion of the KCC2a isoform to the total KCC2 (KCC2a+KCC2b) protein expression in maturing cortical neurons, we used the previously developed method of running of KCC2a protein standards (five serial dilutions) on the same SDS-PAGE alongside with experimental protein lysates (Uvarov et al., 2009). The KCC2a protein standards contain epitopes for both anti-KCC2a and anti-KCC2pan antibodies, which are used for the quantification of KCC2a and total KCC2 (KCC2a+KCC2b) expression, correspondingly. The experimental protein lysates were obtained from dissociated rat cortical neurons cultured for 2, 8, and 14 days *in vitro* (DIV) (n=3 independent cultures for each time point), and the KCC2a and total KCC2 levels were assayed by Western blot using the corresponding antibodies (Fig. 1A). The developmental expression profiles for KCC2a and KCC2 total were normalized to  $\beta$ -tubulin and plotted relative to the total KCC2 expression at DIV2. In agreement with previous reports (Ludwig et al., 2003; Fiumelli, Cancedda, Poo, 2005; Zhu, Lovinger, Delpire, 2005; Khirug et al., 2005; Leonzino et al., 2016), the total KCC2 expression increased ~5-fold during the first week (p<0.001, Student's t-test, n=3) and ~3-fold during the second week in culture (between DIV8 and DIV14, p<0.001, Student's t-test, n=3). Even though KCC2a levels also increased during the two weeks in culture, the upregulation was not so pronounced (~3.5-fold for the 1<sup>st</sup> week, p=0.076; and ~2-fold for the 2<sup>nd</sup> week, p=0.046) compared to the total KCC2 levels (Fig. 1B). The relative proportion of KCC2a to the total KCC2 protein expression was ~40 % in DIV2, ~30 % in DIV8, and ~20 % in DIV14 dissociated cortical cultures (Fig. 1B). We also analyzed the expression of SPAK kinase, which is known to regulate the transport activity of KCC2. SPAK levels rose strongly (~4-fold) between DIV2 and DIV8 points (p=0.04, Student's t-test), but stabilized (p=0.67, Student's t-test) during the second week (Fig. 1B). Thus, the proportion of KCC2a in the total KCC2 expression decreases gradually during two weeks in culture, while SPAK expression increases mostly during the first week. The protein data are in a good agreement with developmental profiles of the KCC2a and KCC2 total mRNA levels between DIV2 and DIV14 time points in dissociated cortical cultures, as measured by quantitative real-time PCR (Fig. 1C). The developmental expression profiles for KCC2a and KCC2 total were normalized to GAPDH and plotted relative to the total KCC2 expression at DIV2. KCC2a mRNA levels increased significantly between DIV2 and DIV8 (~3.5-fold, p<0.001, Student's t-test, n=4), but not later between DIV8 and DIV14 (~1.5-fold, p>0.05, Student's t-test, n=4). In contrast to KCC2a, the upregulation kinetics of the KCC2pan mRNA levels was pronounced during the whole time interval (DIV2 to DIV8: ~3-fold, p<0.001, Student's t-test, n=4; DIV8 to DIV14: ~2-fold, p<0.001, Student's t-test, n=4).

### 2.2 KCC2a overexpression promotes active chloride extrusion and increases $E_{GABA}$ gradient in cultured neurons

The finding that KCC2a isoform constitutes only ~20 % (or less) of the total KCC2 expression in the two-week-old cortical cultures could explain why  $[Cl^-]_i$  remains unchanged in the cultured KCC2b-deficient cortical neurons (Zhu, Lovinger, Delpire, 2005). Indeed, developmental downregulation of  $[Cl^-]_i$  by 15 mM in the wild-type cortical cultures during the

same time interval (Zhu, Lovinger, Delpire, 2005) is normally accompanied by robust 4-5 fold upregulation of the total KCC2 expression (Ludwig et al., 2003; Fiumelli, Cancedda, Poo, 2005; Uvarov et al., 2006). Previous studies have also demonstrated that exogenous overexpression of KCC2b in immature neurons shifts the  $E_{GABA}$  reversal potential by ~20 mV to more negative values, indicating that high level of KCC2 is a prerequisite for the hyperpolarizing GABA responses (Chudotvorova et al., 2005; Liu, Neff, Berg, 2006; Titz, Sammler, Hormuzdi, 2015). Therefore, we asked whether KCC2a overexpression is sufficient to induce the larger  $E_{GABA}$  gradient in KCC2-knockout cortical neurons.

To assess the KCC2a extrusion activity, we used whole-cell patch-clamp recordings from soma under a constant  $Cl^-$  load via a somatic patch pipette (Khirug et al., 2005). Each neuron was stimulated by GABA (uncaging by UV-mediated focal photolysis) at two locations: a dendritic location and at the soma (Fig. 2A). Throughout the experiment, NKCC1 was blocked with 10  $\mu$ M bumetanide, action potentials with 1  $\mu$ M TTX, and GABA<sub>B</sub> receptors with 1  $\mu$ M CGP 55845. The difference between the recordings after stimulations at the soma and dendrite locations ( $E_{GABA}$  somatodendritic gradient) can be attributed to  $Cl^-$  extrusion by KCC2, which leads to the more negative  $E_{GABA}$  values in the dendrite relative to the soma. For our experiments, we used dissociated hippocampal cultures derived from mouse embryos deficient for both KCC2 isoforms (Tornberg et al., 2005). One-week-old KCC2-null neuronal cultures were cotransfected with KCC2a and EGFP constructs and analyzed two days after the transfection. Strong KCC2 expression in the EGFP+KCC2 cotransfected neurons was confirmed by immunostaining with KCC2pan antibody (Fig. 2B). Efficiency of the chloride extrusion mediated by KCC2a isoform in the EGFP+ neurons was assessed by measuring the somatodendritic gradient of reversal potential  $E_{GABA}$  (Fig. 2C). As a control, we used KCC2-null cultures cotransfected with just an empty vector and EGFP. Resting membrane potential was estimated to be about -65 mV in both groups. Imposed  $E_{GABA}$  gradient was significantly larger ( $p < 0.003$ , Student's t-test) in the KCC2a-transfected neurons ( $-0.079 \pm 0.007$  mV/ $\mu$ m,  $n=6$ ) compared to neurons transfected with the empty vector ( $-0.034 \pm 0.009$  mV/ $\mu$ m,  $n=9$ ) (Fig. 2D). Thus, KCC2a isoform can mediate effective chloride extrusion resulting in the significantly augmented somatodendritic  $E_{GABA}$  gradient in the dissociated neuronal cultures.

### ***2.3 KCC2a overexpression attenuates depolarizing GABA<sub>A</sub> responses in cultured neurons***

Since exogenous KCC2a overexpression in cultured neurons affected  $E_{GABA}$  somatodendritic gradient, we asked whether it could also induce a shift in responses of GABA<sub>A</sub> receptors from depolarizing to hyperpolarizing. To address this question, we recorded calcium responses after application of GABA<sub>A</sub> receptor agonist muscimol to the neuronal cultures. The rationale for that experiment was that the depolarizing GABA<sub>A</sub> responses could directly activate voltage-gated calcium channels, and thus could result in the increased intracellular calcium levels (Leinekugel et al., 1995). To avoid the laborious preparation of KCC2-null cultures, we used wild-type neuronal cultures, but measured muscimol-responses at DIV6 when endogenous KCC2 expression is still low (Ludwig et al., 2003; Khirug et al., 2005; Fiumelli, Cancedda, Poo, 2005; Uvarov et al., 2006), and GABA<sub>A</sub> responses are predominantly depolarizing (Chudotvorova et al., 2005; Khirug et al., 2005). In these and subsequent experiments of this study, we used dissociated rat cortical cultures as the major model system. The cultures were transfected with a plasmid expressing either one of the KCC2 isoforms or just an empty vector as a control. EGFP-expressing construct was cotransfected to designate targeted neurons (Fig. 3A). Calcium transients were recorded using Fura-2 AM calcium imaging protocol in EGFP-positive as well as in EGFP-negative neurons after application of 50  $\mu$ M GABA<sub>A</sub> receptor agonist muscimol (Fig. 3B). After washing out muscimol, the extracellular solution with zero potassium concentration was applied and  $Ca^{2+}$  responses were recorded. It has been reported

previously that the extracellular solution with the low potassium concentration ( $[K^+]_o < 0.2$  mM) was able to induce  $Ca^{2+}$  responses in glial cells but not in neurons (Dallwig, Vitten, Deitmer, 2000; Dallwig and Deitmer, 2002). Thus, we used this step to distinguish neurons and astrocytes. Finally, the solution with low potassium was replaced with extracellular solution containing 50 mM KCl and  $Ca^{2+}$  responses were recorded to confirm neuronal vitality. Only those cells that responded to 50 mM KCl, but not to zero  $[K^+]_o$  application, were taken into account for further analysis.

Above 60 % of neurons transfected with the empty vector ( $66 \pm 4$  %,  $n=35$ ) responded with  $Ca^{2+}$  transients upon muscimol application (Fig. 3C), and this ratio was similar to that detected in untransfected cells ( $70 \pm 4$  %,  $n=358$ ). These results indicate that the endogenous KCC2 activity in the majority of one-week-old cultured cortical neurons was not high enough to maintain the low  $[Cl^-]_i$  level required for hyperpolarizing GABA responses. Overexpression of either KCC2a or KCC2b isoform caused a dramatic decrease in the fraction of responding neurons down to ~15 % (KCC2a:  $13 \pm 8$  %,  $n=28$  neurons; KCC2b:  $13 \pm 7$  %,  $n=25$ ) (Fig. 3C). There were no significant difference between KCC2a or KCC2b isoforms, while the difference for both KCC2 variants compared to vector (or untransfected) was significant ( $p < 0.001$ , ANOVA, Bonferroni multiple comparisons test). Thus, both KCC2 variants efficiently ceased the depolarizing responses of GABA<sub>A</sub> receptors. These results ensured that the KCC2a isoform is active in transfected cultured neurons and can reduce the intracellular chloride concentration to the level sufficient for attenuating the depolarizing responses of the GABA<sub>A</sub> receptors.

#### **2.4 Subcellular distribution and membrane localization of the KCC2 isoforms in cultured neurons**

Even though the exogenous KCC2a promotes chloride extrusion in the KCC2-null neurons (Fig. 2) as well as in the immature wild-type neurons (Fig. 3), functionality of the endogenous KCC2a cannot be concluded solely based on overexpression experiments. For example, the forced KCC2a overexpression may overcome putative mechanisms that normally prevent KCC2a trafficking to the neuronal plasma membrane. To assess the functionality of the endogenous KCC2 isoforms, their subcellular distribution and surface expression was examined in two-week-old dissociated rat cortical cultures by immunostaining with the KCC2a and KCC2b antibodies (Fig 4A). At that time point, KCC2b staining was observed in all neurons, and in about half of them KCC2b signal was observed nearby the plasma membrane, i.e., the signal outlined the soma and proximal dendrites while the cytoplasm was only weakly labeled. In contrast, KCC2a-specific antibodies did not reveal any near-surface expression, and KCC2a immunoreactivity was detected exclusively in the intracellular compartments (Fig. 4A). These data are in agreement with our previous report that failed to detect endogenous KCC2a immunoreactivity at the neuronal plasma membrane *in vivo* in several brain regions with high KCC2a expression (Markkanen et al., 2014).

Since biotinylation assay is an established method to assess surface expression of membrane proteins, we used it to compare the membrane expression of KCC2a and KCC2b variants in 2-week-old cortical neurons. Biotin labeling and subsequent Western blot analysis with KCC2a and KCC2b antibodies demonstrated that the relative surface representation of KCC2a and KCC2b isoforms (monomers) was about 40 % of the total expression level for each of the isoforms (Fig. 4B and 4C). Neuronal  $\beta$ -tubulin protein, known to be exclusively cytoplasmic, was not detected in the biotinylated fraction, proving correctness of our biotinylation procedure.

Taken together, the immunostaining data show that both KCC2a and KCC2b are consistently observed in neuronal soma and dendrites. In two-week-old cultures, KCC2b but not KCC2a immunoreactivity is observed nearby the plasma membrane surface of soma and dendrites. Yet, the biotinylation experiments clearly indicate that both isoforms are expressed to similar extent at the neuronal plasma membrane. This discrepancy between the immunostaining and biotinylation data suggests that the N-terminal epitope of KCC2a may be masked at the plasma membrane.

### ***2.5 KCC2a expression at the cell surface is detected by the KCC2a antibody in certain brain areas***

In our previous study, we examined the KCC2a subcellular localization in several areas of adult mouse CNS with high KCC2a expression (brainstem, midbrain, and spinal cord), but failed to observe clear plasma membrane localization of the KCC2a immunoreactivity, whereas KCC2b labeling was observed nearby somatic plasma membrane in virtually all analyzed regions (Markkanen et al., 2014). In the current study, we analyzed KCC2a surface expression in additional brain areas with medium level of KCC2a expression. Brain sections of wild-type, PFA-fixed adult mice were double-labelled with KCC2a and KCC2b antibodies, and KCC2a expression was clearly seen in the subiculum, a part of the hippocampal formation, but not in the nearby CA1 area (Fig. 5A). In contrast, KCC2b staining was found throughout hippocampus formation, as reported previously (Fig. 5A). Confocal images revealed KCC2a labeling nearby neuronal soma surface in the subiculum and a somewhat less clear signal at the surface of hypothalamic neurons (Fig. 5B). In both cases, KCC2b labeling was clearly detected nearby the soma surface. Similar to our previous data from pons and deep cerebellar nuclei (Markkanen et al., 2014), KCC2b but not KCC2a labeling was detected at the plasma membrane of neuronal somas in the medulla oblongata (Fig. 5B). KCC2b immunostaining was localized at the neuronal plasma membrane in all brain areas (including hippocampus and cortex) and similarly in KCC2a-deficient (Suppl. Fig. 1) and wild-type mice (Fig. 5 and Suppl. Fig. 2). Thus, different regions of the adult mouse brain demonstrate different levels of KCC2a plasma membrane labeling varying from the very low in the brainstem to the substantially high in the hypothalamus and subiculum. In contrast, KCC2b immunoreactivity is seen at the neuronal soma surface practically in all analyzed brain areas.

### ***2.6 SPAK reveals higher affinity to KCC2a compared to KCC2b***

One possible explanation for the KCC2a epitope masking is the canonical SPAK/OSR1 binding motif found in the N-terminus of the KCC2a isoform (Uvarov et al., 2007). The canonical SPAK/OSR1 binding motif RFX(V/I) is present in at least one splice variant of each mammalian CCC family member, except KCC1 (Fig. 6A). To examine whether SPAK interacts differentially with KCC2a isoform carrying the RFX(V/I) motif, and KCC2b, which lacks such motif, we used co-immunoprecipitation assay. The hemagglutinin-tagged SPAK protein (HA-SPAK) was co-expressed with either KCC2a or KCC2b in HEK293 cells; as a negative control, SPAK was co-expressed with an empty expression vector. The protein complexes were immunoprecipitated using KCC2pan antibody, which recognizes C-terminal domain common for both isoforms. Since KCC2a and KCC2b isoforms possess identical C-termini, we assumed that the precipitation conditions would be similar for both KCC2 isoforms. Indeed, KCC2a and KCC2b proteins were both efficiently immunoprecipitated by KCC2pan antibody, while no KCC2 was detected in the negative control lysate (empty expression vector) (Fig. 6B, the first top panel), thus corroborating the absence of endogenous KCC2 expression in HEK293 cells (Payne, Stevenson, Donaldson, 1996; Williams et al., 1999). In agreement with presence of SPAK-binding motif in KCC2a but not in KCC2b isoform, immunoblotting with anti-HA antibody revealed the strong signal corresponding to the

co-precipitated SPAK in lysates obtained from HEK293 cells transfected with KCC2a (Fig. 6B, the second top panel). In contrast, only weak background signals were observed in the KCC2b and the control lysates. Additional analysis of input samples confirmed equal SPAK expression in all three samples; KCC2a and KCC2b expression in the input samples also were similar (Fig. 6B, the third and fifth panels).

To confirm above results, we reversed co-immunoprecipitation assay and used anti-HA antibody to precipitate protein complexes from the same HEK293 lysates (Fig. 6C). Precipitation with the anti-HA antibody was not as effective as with the KCC2pan antibody, yet detectable HA-SPAK enrichment was observed (Fig. 6C, the first top panel). The precipitated complexes contained KCC2a, as revealed by immunoblotting with KCC2a antibody (Fig. 6C, the second top panel), indicating that SPAK binds KCC2a in the heterologous expression system. The KCC2pan antibody was also able to detect a clear band corresponding to the dimeric KCC2a isoform, but only a more diffuse band in the KCC2b-expressing sample (Fig. 6C, the third panel). Detection of the monomeric KCC2 isoforms in the immunoprecipitated complexes was prevented by the previously described irreversible KCC2 aggregation upon heating protein lysates at temperatures higher than 70 °C (Blaesse et al., 2006; Uvarov et al., 2009). Indeed, the procedure of stripping the protein complexes from agarose beads after immunoprecipitation includes heating of the precipitated samples at 95 °C for 5 minutes, while the notable KCC2 aggregation starts already at temperatures above 60 °C that leads to fading of the KCC2 monomeric band (Suppl. Fig. 3). Additional analysis of the input samples revealed equal levels of SPAK in all lysates, and similar expression level for KCC2a and KCC2b proteins in the lysates transfected with the corresponding expression vectors (Fig. 6C, Input panels). Thus, co-immunoprecipitation data demonstrated that SPAK interaction with KCC2a, which has SPAK/OSR1 binding consensus, is substantially stronger than that with KCC2b, which lacks such motif.

### ***2.7 SPAK differently regulates kinetic activity of KCC2a and KCC2b isoforms in HEK293 cells***

Previous reports have pointed at the important role of SPAK and OSR1 kinases in regulation of CCC family members: both kinases are known to inhibit KCC proteins and to activate NCC and NKCC proteins (Alessi et al., 2014). Given the differential interaction of SPAK with KCC2a and KCC2b isoforms, we asked whether this could also result in differential regulation of the chloride transport activity of the KCC2 variants by SPAK. To answer this question, we utilized the functional  $^{86}\text{Rb}$  assay in HEK293 cells, which are known to express endogenously KCC1, KCC4, and NKCC1 proteins (Xu et al., 1994; Simard et al., 2007), but neither KCC2a nor KCC2b isoforms (Payne, 1997; Uvarov et al., 2009). Functional  $^{86}\text{Rb}$  assay is a direct method for measuring the activity of potassium channels and transporters, since  $\text{K}^+$  cation can be substituted by its radioactive congener -  $^{86}\text{Rb}^+$  (Bartschat and Blaustein, 1985). Thus, the transport activity can be assessed by quantifying the accumulation of radioactive  $^{86}\text{Rb}$  in the cells. Rubidium assay was performed to measure the influx (not efflux) mode of the KCC2 transport activity as described previously (Payne, 1997; Uvarov et al., 2007). The inversed mode of KCC2 transport activity is induced by increasing the extracellular  $\text{K}^+$  (or  $^{86}\text{Rb}^+$ ) concentration up to 5 mM (Payne, 1997).

We transiently transfected HEK293 cells with constructs encoding either KCC2a or KCC2b isoforms and confirmed their expression at the plasma membrane by immunostaining with antibodies to KCC2pan (red) (Fig. 7A; nuclei are labeled by DAPI (blue)). The  $^{86}\text{Rb}^+$  flux was measured with and without furosemide (2 mM), a well-known inhibitor of KCC cotransporters, to determine the furosemide-sensitive component of the K-Cl transport activity mediated by the

KCC2a and KCC2b variants. Bumetanide (10  $\mu$ M), a potent inhibitor of the endogenously expressed NKCC1 protein (Xu et al., 1994), was added into all flux solutions to exclude NKCC1 impact on  $^{86}\text{Rb}$  uptake. Transient overexpression of either KCC2 variant increased the furosemide-sensitive  $^{86}\text{Rb}$  uptake by  $\sim 35$ -fold compared to control HEK293 cells transfected with empty vector (Fig. 7B). This is in agreement with previous results showing that KCC2a and KCC2b proteins mediate similar  $^{86}\text{Rb}$  uptake in isotonic conditions (Uvarov et al., 2007). Co-expression of SPAK with KCC2a isoform decreased the furosemide-sensitive  $^{86}\text{Rb}$  uptake by  $\sim 20\%$  ( $81 \pm 6\%$ ,  $p < 0.05$ , one-sample t-test,  $n=6$ ) compared to uptake by cells cotransfected with KCC2a and a control empty vector (Fig. 7C). In contrast, SPAK co-expression with KCC2b did not change the furosemide-sensitive  $^{86}\text{Rb}$  uptake compared to uptake by control cells transfected with KCC2b only ( $109 \pm 9\%$ ,  $p > 0.05$ , one-sample t-test,  $n=6$ ).

It has been shown previously that SPAK and OSR1 kinases can be activated by low  $[\text{Cl}^-]$  (Gagnon, England, Delpire, 2006a; Richardson et al., 2008; de Los Heros et al., 2014). This suggests that the endogenous SPAK/OSR1 in HEK293 cells could be activated upon KCC2a/KCC2b transfection. To test whether KCC2a and KCC2b isoforms are regulated by endogenous SPAK/OSR1 in HEK293 cells, we overexpressed the kinase-inactive K101R mutant form of SPAK (DNPAK), which can interact with SPAK/OSR1-binding motif in target proteins, but is unable to phosphorylate the targets (Dowd and Forbush, 2003). As expected, DNPAK overexpression strongly (3.2-fold) enhanced the KCC2a-mediated furosemide-sensitive  $^{86}\text{Rb}$  uptake ( $220 \pm 70\%$ ,  $p < 0.05$ , Student's t-test,  $n=6$ ) relative to the cells transfected with KCC2a construct only (Fig. 7C). Interestingly, DNPAK also upregulated (2.6-fold) the KCC2b mediated furosemide-sensitive  $^{86}\text{Rb}$  uptake ( $160 \pm 20\%$ ,  $p < 0.01$ , Student's t-test,  $n=6$ ).

### 3. Discussion

The main findings of this paper are: 1) overexpressed KCC2a isoform is active in cultured neurons, 2) endogenous KCC2a is present at the neuronal plasma membrane but its N-terminal epitope can be masked, and 3) SPAK binds and inhibits KCC2a.

The functionality of the KCC2b isoform is well-established (Rivera et al., 1999), but data regarding the KCC2a role in neurons has remained elusive. Importance of KCC2a is inferred from the comparisons of mice lacking both KCC2 isoforms that cannot maintain respiratory rhythm and die immediately after birth (Hubner et al., 2001), and mice deficient for the KCC2b isoform (and retaining KCC2a) that survive postnatally for three weeks (Woo et al., 2002). Yet, adult KCC2a-deficient mice show no obvious gross neurological phenotype (Markkanen et al., 2014). In this study, we have examined three working hypotheses to explain this apparent controversy: (1) KCC2a protein expression in two-week-old cultures may be too low to affect the intracellular chloride concentration, (2) KCC2a traffic to the plasma membrane may be impeded, and (3) KCC2a transport activity may be inhibited by mechanisms that have been shown previously to regulate activity of KCC2 (Alessi et al., 2014; Kahle and Delpire, 2016).

First, we established that the relative KCC2a expression is indeed low in the dissociated cortical neurons and constitutes only about 20 % of the total KCC2 expression in two-week old cultures. Previous reports have estimated the relative contribution of KCC2a to the total KCC2 expression in the mouse cortex as 60 % at birth, gradually decreasing to ~15 % in two-week old pups, and to ~10 % in adult mice (Woo et al., 2002; Uvarov et al., 2007; Uvarov et al., 2009). Similar values (~20 %) were observed in the mouse spinal cord during first postnatal week (Stil et al., 2011). This low level of expression could explain why the remaining KCC2a expression in the KCC2b-deficient mice is not sufficient for maintaining the hyperpolarizing responses of glycine receptors in spinal motoneurons (Stil et al., 2011) or GABA<sub>A</sub> receptors in cortical neurons (Zhu, Lovinger, Delpire, 2005), resulting in seizures and lethality three weeks after birth (Woo et al., 2002). Indeed, the developmental shift in the GABA<sub>A</sub> receptor responses is accompanied by the robust increase in the KCC2 expression in maturing neurons (Rivera et al., 1999; Fiumelli, Cancedda, Poo, 2005; Zhu, Lovinger, Delpire, 2005; Khirug et al., 2005; Uvarov et al., 2006; Leonzino et al., 2016), mainly due to the upregulation of the KCC2b isoform (Uvarov et al., 2009).

KCC2b overexpression in immature cultured neurons produces a substantial negative shift in the GABA reversal potential and strongly attenuates GABA-elicited calcium responses (Chudotvorova et al., 2005; Lee et al., 2005; Liu, Neff, Berg, 2006). In the present study, we found that the overexpression of KCC2a increased the somatodendritic  $E_{\text{GABA}}$  gradient in the dissociated hippocampal neurons derived from the KCC2-null embryos. Moreover, KCC2a overexpression in immature wild-type cortical neurons decreased the fraction of neurons that showed muscimol-induced  $\text{Ca}^{2+}$ -transients. Taken together, overexpressed KCC2a, similar to KCC2b, is active in neuronal cells under isotonic conditions. This corroborates previous observations attributing the unique ability of KCC2 to work in isotonic conditions to the C-terminal ISO domain (Mercado et al., 2006; Acton et al., 2012) that is identical in KCC2a and KCC2b isoforms.

Functionality of the endogenous KCC2a cannot be concluded solely based on overexpression experiments. For example, the forced KCC2a overexpression may overcome putative control mechanisms that normally prevent KCC2a trafficking to the neuronal plasma membrane. Our previous report failed to detect endogenous KCC2a immunoreactivity at the neuronal plasma membrane in several brain regions with high KCC2a expression (Markkanen et al., 2014). Similarly, in the present study, endogenous KCC2a immunoreactivity was detected mainly

intracellularly in cortical neurons cultured for two weeks, while KCC2b immunoreactivity was predominantly observed nearby the plasma membrane. Similar results were observed in cultured mouse hippocampal neurons (Suppl. Fig. 4). Surprisingly, in contrast to the immunostaining data, our biotinylation assays clearly showed that both KCC2 isoforms are similarly present at the plasma membrane of two-week-old cultured cortical neurons. This suggests that the KCC2a N-terminal epitope, which is recognized by the KCC2a antibody, could be masked. To test this hypothesis further, we used KCC2b-deficient mice (Woo et al., 2002), in which KCC2a remains the only expressed KCC2 isoform (Uvarov et al., 2007). Immunostainings of brain sections obtained from these mice with KCC2pan antibody, which recognizes the common C-terminus of KCC2 (Williams et al., 1999), indeed demonstrated immunoreactivity nearby the plasma membrane, while the KCC2a immunoreactivity was still intracellular (Suppl. Fig. 5). We re-examined our previous immunostaining data obtained with KCC2a and KCC2b antibodies from brain sections of adult wild-type mice (Markkanen et al., 2014). This analysis confirmed our previous observations that KCC2a immunoreactivity is predominantly intracellular in most analyzed brain areas. However, we did find clear near-surface expression of KCC2a in the subiculum and less prominent near-surface expression in some hypothalamic areas. In contrast, KCC2b immunostaining was localized at the neuronal plasma membrane in all brain areas and similarly in KCC2a-deficient (Suppl. Fig. 1) as in wild-type mice (Fig. 5 and Suppl. Fig. 2). The reason for the KCC2a epitope masking remains unclear at present, but could for example be due to heterodimerization since KCC2a and KCC2b immunoreactivities clearly overlap in several areas as seen in confocal images presented in Fig. 5B. Previous reports have shown that KCC2a and KCC2b isoforms can form oligomers (Blaesse et al., 2006; Uvarov et al., 2009; Mahadevan et al., 2014). Also clustering in lipid rafts may play a role in the KCC2a epitope masking as previous reports have shown that KCC2 can be detected in lipid rafts (Watanabe et al., 2009; Hartmann et al., 2009).

Epitope masking could also result from expression of protein(s) that bind the N-terminal epitope. An obvious candidate for the KCC2a epitope masking is the Ste20-related proline alanine rich kinase (SPAK alias STK39). The binding motif RFX(V/I) for SPAK (or its homologue oxidative stress responsive kinase, OSR1) is located in the unique N-terminal part of the KCC2a (Uvarov et al., 2007). In agreement with existence of the motif in KCC2a but not in KCC2b, we show that SPAK binds preferentially KCC2a but not KCC2b isoform in the heterologous HEK293 expression system. Although the SPAK binding motif (residues 4-7) is outside the KCC2a antibody binding epitope (residues 20-40), the dimeric domain-swapped structures of SPAK and OSR1 kinases (Lee, Cobb, Goldsmith, 2009; Taylor et al., 2015) and their reported crystal structures in complex with RFXV containing peptides (Villa et al., 2007; Taylor et al., 2015) suggest that the epitope could become sterically hidden by the large dimeric SPAK kinase complex. The heterogeneous expression pattern of SPAK protein (Ushiro et al., 1998; Johnston et al., 2000; Piechotta et al., 2003) and mRNA (Allen Brain Atlas) in the mouse brain could also explain why KCC2a immunoreactivity is detected nearby neuronal surface in some but not other brain regions. Testing this hypothesis by comparing the co-localization of KCC2a and SPAK was hindered by lack of good antibodies suitable for immunohistochemistry. However, analysis of SPAK mRNA expression pattern in adult mouse brain revealed a low expression level of SPAK in subiculum and hypothalamus, while much stronger expression could be seen in deep cerebellar nucleus or medulla (Suppl. Fig. 6), thus supporting our hypothesis. In addition, SPAK can be rapidly translocated from cytosol into cytoskeletal fraction under osmotic, oxidative or high temperature stress (Ushiro et al., 1998; Tsutsumi et al., 2000). We speculate that this regulation of SPAK distribution between the cytosol and cytoskeleton could also be involved in the differential plasma membrane expression of KCC2a

immunoreactivity in different brain regions. However, the physiological relevance of this remains to be studied.

The  $\alpha 2$ -subunit of  $\text{Na}^+/\text{K}^+$ -ATPase (NKA) is also a possible candidate for the role of the N-terminal “masker”, as previous data have demonstrated physical interaction between KCC2 and  $\alpha 2$ -subunit of NKA (Ikeda et al., 2004). Ikeda and coauthors have also highlighted a similarity between KCC2 and NKA expression patterns. In their co-IP experiments the authors used an antibody produced against a short C-terminal fragment of KCC2 (CDNEEKPEEEVQLIH, 961-975 aa of the mouse KCC2 sequence) identical in KCC2a and KCC2b, thus leaving open the question which KCC2 isoform interacts with NKA. Interestingly, another member of the K-Cl cotransporter subfamily – KCC3a – has recently been shown to interact with the  $\alpha 1$ -subunit of NKA (Fujii et al., 2008). Moreover, KCC2 and NKA have been shown to colocalize in chicken heart, where KCC2a is the only expressed isoform (Antrobus, Lytle, Payne, 2012).

Since OSR1 protein expression level is much lower compared to SPAK in mouse brain (Geng, Hoke, Delpire, 2009), we concentrated on KCC2 regulation by SPAK. To study regulation of the KCC2a and KCC2b transport activities by SPAK, we chose HEK293 cells, which have been extensively used for studying SPAK-mediated regulation of cation-chloride cotransporters. HEK293 cells express endogenously KCC1, KCC4, and NKCC1 proteins (Xu et al., 1994; Simard et al., 2007), but neither KCC2a nor KCC2b (Payne, 1997; Uvarov et al., 2009). Previously we found that exogenous KCC2a overexpression results in the furosemide-sensitive efficient chloride flux in HEK cells (Uvarov et al., 2007). In the present study, we confirmed trafficking of both KCC2 isoforms to the plasma membrane after exogenous overexpression and significant increase of the furosemide-sensitive  $^{86}\text{Rb}$  uptake. The potent NKCC1 inhibitor bumetanide was added to all solutions to exclude NKCC1-mediated  $^{86}\text{Rb}$  flux. The impact of the endogenous KCC1 and KCC4 cotransporters was low as determined from values of  $^{86}\text{Rb}$  flux in the control cells transfected with empty vector. It is important to note that SPAK and OSR1 kinases, as well as their upstream kinase WNK1, are expressed endogenously in HEK293 cells (Vitari et al., 2006; Rinehart et al., 2009). Thus, it is possible that overexpressed KCC2a (or KCC2b) will be exposed to regulation mediated by endogenous SPAK. This could partly explain the rather moderate inhibition (~20 %) of the furosemide-sensitive  $^{86}\text{Rb}$  flux after the exogenous SPAK overexpression in the HEK293 cells co-expressing KCC2a, compared to the cells overexpressing KCC2a only. The relatively mild effect of the exogenous SPAK overexpression on the KCC2a activity in our experiments could also be caused by the absence of the MO25 coactivator, which has been reported to dramatically (~100-fold) enhance the ability of SPAK/OSR1 to directly phosphorylate KCC2a and other cotransporters in biochemical assays (Filippi et al., 2011; de Los Heros et al., 2014). Nevertheless, in contrast to KCC2a, we did not detect any effect of SPAK overexpression on the transport activity of the KCC2b isoform. Although SPAK expression (in oocytes) has been shown previously to inhibit KCC2b transport activity in hypotonic/low chloride conditions (Gagnon, England, Delpire, 2006b), we speculate that since the experiment was performed in isotonic solution (and without adding WNKs or MO25 coactivator), SPAK activity was probably relatively low, and thus inhibition of KCC2b was not detected. Previous data have also failed to reveal KCC2b inhibition in isotonic conditions after SPAK overexpression in the absence of WNKs (Gagnon, England, Delpire, 2006b).

Multiple serine ( $\text{Ser}^{78}$ ,  $\text{Ser}^{83}$ ) and threonine ( $\text{Thr}^6$ ,  $\text{Thr}^{77}$ ,  $\text{Thr}^{92}$ ,  $\text{Thr}^{929}$ , and  $\text{Thr}^{1030}$ ) residues in KCC2a isoform have been reported as phosphorylation targets of the SPAK kinase (de Los Heros et al., 2014). Since KCC2a possess only 40 unique amino acids, all these phosphorylation sites except  $\text{Thr}^6$  are also present in KCC2b. Thus, both KCC2 isoforms could

possibly be phosphorylated by endogenous SPAK in HEK293 cells even without exogenous SPAK overexpression. Consistent with this it has been shown previously that the C-terminal part of KCC2b isoform is affected by WNK-SPAK pathway (Inoue et al., 2012; de Los Heros et al., 2014; Friedel et al., 2015), even though the KCC2b isoform lacks the SPAK-binding motif.

To test whether KCC2a and KCC2b isoforms are regulated by endogenous SPAK/OSR1 in HEK293 cells, we overexpressed the dominant negative SPAK (DNPAK) (Dowd and Forbush, 2003). This DNPAK contains a single amino acid substitution (K101R) within the catalytic domain that impairs its kinase activity. Thus, DNPAK can bind proteins at the same sites as SPAK, but cannot phosphorylate them. The exact outcome of the DNPAK binding to target proteins is not obvious except that it prevents their phosphorylation. For example, possible conformation changes of the target proteins after DNPAK binding cannot be excluded.

In our experiment, DNPAK overexpression strongly enhanced the furosemide-sensitive  $^{86}\text{Rb}$  uptake mediated by both KCC2a and KCC2b (Fig. 7C). The results imply that endogenous SPAK/OSR1 in HEK293 cells are active and inhibit the function of both KCC2 isoforms (and possibly the function of other KCCs that are present in HEK cells), and when DNPAK is expressed, this inhibitory effect of endogenous SPAK would be prevented, leading to increased  $^{86}\text{Rb}$  uptake. Another possible explanation for the disinhibition of both KCC2 isoforms by DNPAK is the SPAK-independent effect of WNK3 on the KCC2 phosphorylation status (e.g. via repression of protein phosphatases). In this case, the overexpressed DNPAK could work as a scaffold for endogenous WNK3 (via the SPAK-binding motifs present in WNKs). Consistent with this, an increase in the transport activity of KCC2b has been observed previously after overexpression of DNPAK in *Xenopus* oocytes (Gagnon, England, Delpire, 2006b)

#### 4. Conclusions

Taken together, our data suggest a more efficient regulation of the KCC2a than KCC2b isoform by SPAK. The different interaction of KCC2a and KCC2b isoforms with SPAK could explain the open question why KCC2 in adult brain is less subject to inhibitory phosphorylation by SPAK than that in immature brain, despite developmental upregulation of SPAK (Inoue et al., 2012; Friedel et al., 2015). We propose that the KCC2a isoform is an important component of the intricate system regulating intracellular chloride concentration in neurons. Future *in vivo* experiments will be required to study the phosphorylation of endogenous KCC2 isoforms, and to elucidate the physiological role of SPAK binding. Whether the SPAK interaction with KCC2a is responsible for preventing epitope recognition of the KCC2a-specific antibody will also be addressed in future studies.

## 5. Experimental Procedures

### 5.1 Expression constructs

KCC2a and KCC2b expression constructs were described previously (Uvarov et al., 2007). HA-tagged SPAK (HA-SPAK) and dominant negative, kinase-inactive K101R form of SPAK (DN-SPAK) (Dowd and Forbush, 2003) were a kind gift of Dr. B. Forbush.

### 5.2 Neuronal cultures

Standard dissociated hippocampal neuronal cultures were prepared from *embryonic* day 17 (E17) mice as described previously (Banker and Goslin, 1998) with small modifications. Briefly, hippocampal cells were dissociated by enzymatic treatment (0.25 % trypsin for 15 min at 37 °C) and plated (50,000 cells/cm<sup>2</sup>) on poly-DL-ornithine-coated coverslips (Sigma, St. Louis, MO). The cells were grown in Neurobasal medium containing B27 supplement (Invitrogen, Carlsbad, CA) preincubated on astroglial cultures for 24 h. Standard dissociated cortical cultures were prepared from embryonic day 18 (E18) rats similar to the protocol described above for the hippocampal neuronal cultures. Neurons were plated (100,000 cells/cm<sup>2</sup>) on poly-DL-ornithine-coated coverslips (Sigma, St. Louis, MO) and were grown in Neurobasal medium containing B27 supplement, glutamine, and penicillin + streptomycin antibiotics mix (Neurobasal medium and all additives were from Invitrogen/Gibco, Carlsbad, CA).

### 5.3 Mice and rats

All procedures related to a treatment and a care of animals were in accordance with national and international guidelines and approved by the National Animal Experiment Board, Finland. Mice and rats were housed under standard conditions. Rats as well as wild-type NMRI and C57Bl/6JHsd mice of both sexes were obtained from a local breeding center (Experimental Animal Center, University of Helsinki) at different ages. KCC2b-knockout (Woo et al., 2002) and KCC2null mice (Tornberg et al., 2005) have been characterized previously.

### 5.4 KCC2 antibodies

The affinity-purified KCC2a antiserum was produced in rabbits against a 21–amino acid peptide corresponding to the N-terminus of the mouse KCC2a isoform (amino acids 20–40; DPESRRHSVADPRRLPREDVK) (Uvarov et al., 2009). Polyclonal antibodies against the KCC2b isoform were generated in chicken against a 15–amino acid peptide corresponding to the N-terminus of the mouse KCC2b isoform (amino acids 8–22; CEDGDGGANPGDGNP) (Markkanen et al., 2014). The KCC2pan antiserum was raised in rabbits against a recombinant 117–amino acid segment of the C-terminus of rat KCC2 (amino acids 929–1045) common to both KCC2a and KCC2b (Ludwig et al., 2003).

### 5.5 Western blot

Cultured neurons and human embryonic kidney (HEK) 293 cells (CLR-1573, American Type Culture Collection, Manassas, VA) were homogenized in a lysis buffer (50 mM Tris-HCl, 150 mM NaCl, 1 % Triton X-100, 0.5 % deoxycholic acid, 0.1 % SDS, pH 8.0) supplemented with the Complete Protease Inhibitor Cocktail and the PhosStop phosphatase inhibitor cocktail (both from Roche Diagnostics, Mannheim, Germany). Protein concentration was determined using the DC Protein Assay kit (Bio-Rad, Hercules, CA). Protein samples were separated using Criterion XT Precast Bis-Tris gels (Bio-Rad Laboratories Inc, CA) and transferred onto Hybond-ECL nitrocellulose membrane (GE Healthcare, UK). To assess an impact of the KCC2a isoform to the total KCC2 (KCC2a+KCC2b) expression, we used the previously developed method (Uvarov et al., 2009). Briefly, KCC2a protein standards (five serial dilutions) were run on the same SDS-PAGE alongside with experimental protein lysates. The

KCC2a protein standards contained epitopes for anti-KCC2a and anti-KCC2pan antibodies, thus allowing quantification of KCC2a and total KCC2 (KCC2a+KCC2b) expression using standard curves. Blots were probed with rabbit anti-KCC2a (1:2,000) (Uvarov et al., 2009), chicken anti-KCC2b (1:2,000) (Markkanen et al., 2014), rabbit anti-KCC2pan (1:2,000) (Ludwig et al., 2003), rabbit anti-SPAK (1:2,000) (Ushiro et al., 1998) (a kind gift of Dr. H. Ushiro), mouse anti-(neuronal class III  $\beta$ -tubulin) (1:10,000) (BabCO, Berkeley, CA), and mouse monoclonal anti-HA (12CA5) (1:2,000) antibodies with subsequent probing with horseradish peroxidase conjugated goat anti-rabbit IgG (GE Healthcare, UK), goat anti-chicken IgY (Abcam) or goat anti-mouse IgG (DAKO, Denmark) antibodies. Blots were developed with Pierce ECL Western Blotting Substrate (Pierce Biotechnology, IL) and visualized with the luminescent image analyzer LAS-3000 (Fuji Photo Film, Tokyo, Japan). Optical densities of the bands were analyzed with Advanced Image Data Analysis (AIDA) imaging software (Raytest, Straubenhardt, Germany). KCC2a fraction in the total KCC2 protein expression was determined as described previously (Uvarov et al., 2009).

### 5.6 Quantitative RT-PCR

Total RNA was isolated from dissociated rat cortical cultures using RNeasy Plus Mini kit (Qiagen). Typically,  $\sim 0.3$   $\mu$ g of total RNA was reverse-transcribed using Maxima First Strand cDNA Synthesis kit (Thermo Scientific) and a mixture of oligo(dT)<sub>18</sub> and random hexamer primers according to the manufacturer's protocol. The cDNA samples were amplified using the Maxima SYBR Green qPCR kit (Thermo Scientific) and detected via the CFX96 Real-Time PCR Detection System (Bio-Rad). Primers for KCC2a (5'-gccggctcccagggaag-3', 5'-cttctccgtgtccgtgctgtgatg-3'), KCC2pan (5'-tctcaaacagatgcacctcacca-3', 5'-acgtgtctcttcgggaacattga-3'), and glyceraldehyde-3-phosphate dehydrogenase (GAPDH) (5'-cagtgccagctcgtctcata-3', 5'-tggtaccaggcgtccgata-3') quantification were designed with Express v2.0 software (Applied Biosystems) or manually and contained at least one intron in between.

### 5.7 Immunocytochemistry

Hippocampal neuronal cultures were fixed for 10 min in -20 °C cold methanol, washed in phosphate-buffered saline (PBS), and blocked for 1 h at 24 °C in a blocking solution (4 % BSA, 3 % sheep serum, 0.2 % Triton X-100, in PBS). The cells were first incubated in 2 % BSA/1.5 % sheep serum/0.2 % Triton-X100 in PBS containing anti-KCC2pan rabbit polyclonal antibody (1:1,000) at 24 °C for 2 h, washed three times for 10 min with PBS, and then incubated with cyanine 3-conjugated donkey anti-rabbit secondary antibody (1:400) (Jackson ImmunoResearch, West Grove, PA). After three washings for 10 min in PBS and one washing in water, processed coverslips were mounted in Gelvatol (Biomedica, Foster City, CA). Fixation and immunostaining of cortical cultures were performed as described for hippocampal cultures, except that normal donkey serum was used instead of sheep serum. As primary antibodies, anti-KCC2a rabbit (1:1000) and anti-KCC2b chicken (1:1000) polyclonal antibodies were used. Primary antibodies were then detected using cyanine 3-conjugated donkey anti-rabbit (1:400) or cyanine 3-conjugated donkey anti-chicken (1:400), respectively (both secondary antibodies from Jackson ImmunoResearch, West Grove, PA). Coverslips were mounted in Vectashield HardSet Mounting Medium.

### 5.8 Electrophysiological recordings

Standard dissociated hippocampal neuronal cultures were prepared from embryonic day 17 (E17) mice homozygous for the KCC2null mutation (Tornberg et al., 2005) as described above. At DIV8, cells were cotransfected by EGFP with either KCC2a or empty expression vector. Efficiency of Cl<sup>-</sup> extrusion by KCC2 was assessed in DIV10 EGFP-positive neurons as

described previously (Khirug et al., 2005). Briefly, we applied a constant  $\text{Cl}^-$  load (19 mM) via the somatic patch pipette and compared the reversal potential of GABAergic currents ( $E_{\text{GABA}}$ ) after stimulation at the soma to that after stimulation at a dendritic location, approximately 50  $\mu\text{m}$  from soma. GABA was photolysed (by UV-mediated focal photolysis) from a CNB-caged GABA compound (2 mM in the extracellular solution) (Molecular Probes, OR, USA). Diameter of the uncaging spot is  $\sim 10 \mu\text{m}$  as determined previously (Fig. 1D in Khirug et al., 2005). The spreading of GABA to distal areas is in addition significantly decreased by the constant perfusion of the neurons with fresh extracellular solution. Under such conditions, difference between  $E_{\text{GABA}}$  values measured after GABA-uncaging at the soma and at the dendrite (the somato-dendritic  $E_{\text{GABA}}$  gradient) can be attributed to  $\text{Cl}^-$  extrusion by KCC2. Recordings were performed in the extracellular solution (127 mM NaCl, 3 mM KCl, 2 mM  $\text{CaCl}_2$ , 1.3 mM  $\text{MgCl}_2$ , 10 mM D-glucose, and 20 mM HEPES, pH 7.4. at room temperature in the whole-cell voltage-clamp configuration. NKCC1 was blocked throughout the experiments with 10  $\mu\text{M}$  bumetanide, action potentials with 1  $\mu\text{M}$  TTX and GABA<sub>B</sub> receptors with 1  $\mu\text{M}$  CGP 55845 (Tocris, Bristol, UK). Borosilicate glass (Harvard Apparatus, UK) patch pipettes with resistances ranged from 6.5 to 7.5 M $\Omega$  were filled with intracellular solution (18 mM KCl, 111 mM K-gluconate, 0.5 mM  $\text{CaCl}_2$ , 2 mM NaOH, 10 mM D-glucose, 10 mM HEPES, and 2 mM Mg-ATP, 5 mM BAPTA, pH 7.3). Recordings from EGFP-positive neurons with access resistances between 10 and 20 M $\Omega$  were used for analysis. All membrane potential values were corrected for a liquid-junction potential of 10 mV.  $E_{\text{GABA}}$  was derived from the current–voltage (I–V) plot obtained by sequentially clamping the somatic membrane at different voltage levels. I–V curves were normalized with respect to peak  $I_{\text{GABA}}$  at the most negative holding potential ( $V_h$ ) tested. After the experiments, neuronal cultures were fixed in 4 % paraformaldehyde (PFA) and immunostained with rabbit anti-KCC2pan antibodies to demonstrate the level of KCC2 expression in the neurons transfected with the KCC2a expression construct versus non-transfected neurons.

### 5.9 Calcium imaging

Dissociated rat cortical cultures were prepared from E18 embryos and plated (100,000 cells/ $\text{cm}^2$ ) on 35 mm MatTek dishes (MatTek Corporation, MA, USA) with 10 mm glass microwell bottom pre-coated with poly-L-lysine as described above. Cultures were cotransfected at DIV3 with a mix containing EGFP and one of the expression constructs (KCC2a, KCC2b, or empty vector as a control), and  $\text{Ca}^{2+}$  imaging was performed at DIV6 as described previously (Sokka et al., 2007) with small modifications. Conventional wide-field fluorescence microscopy integrated in CellR Olympus IX71 microscope system equipped with a 10x objective and CCD camera (Orca, Hamamatsu, Japan) was used to monitor the muscimol-induced  $\text{Ca}^{2+}$  responses. Cells were loaded with 5  $\mu\text{M}$  calcium indicator Fura-2 acetoxymethyl ester (AM) (Invitrogen) supplied with 0.02 % Pluronic F-127 (Sigma–Aldrich) by incubation at room temperature for 30 min in the extracellular solution (127 mM NaCl, 3 mM KCl, 2 mM  $\text{CaCl}_2$ , 1.3 mM  $\text{MgCl}_2$ , 20 mM HEPES, and 10 mM glucose, pH 7.4). After washing out Fura-2 AM cells were incubated during 20 min for de-esterification, during which the EGFP-positive neurons were identified for subsequent  $\text{Ca}^{2+}$  recordings. To analyze  $\text{Ca}^{2+}$  transient responses in the EGFP-positive as well as in the nearby untransfected cells, intensities of the fluorescent signals collected using a 410 nm dichroic mirror and a 505 nm barrier filter after consecutive excitation of the measured cells at 340 and 380 nm were recorded (Grynkiewicz, Poenie, Tsien, 1985). Changes in  $[\text{Ca}^{2+}]_i$  were expressed as  $\Delta F/F$ , where F is baseline fluorescence level,  $\Delta F$  is the relative change from the base level of the 380 nm component. Due to a relatively low intensity of the 340 nm component for the particular combination of the filters and objective in our experiments, only the 380 nm component was taken for subsequent analysis. A standard protocol included 1 min basal recording, after which

muscimol (50  $\mu$ M) was applied during 1 min through a bath perfusion system. To discriminate between glial cells and neurons, we used a previously described protocol that takes into account their different  $\text{Ca}^{2+}$  responses on application of low external  $[\text{K}^+]$  (Dallwig and Deitmer, 2002). Viability of the recorded cells was assessed in high potassium extracellular solution (80 mM NaCl, 50 mM KCl, 2 mM  $\text{CaCl}_2$ , 1.3 mM  $\text{MgCl}_2$ , 20 mM HEPES, and 10 mM glucose, pH 7.4). Only those neurons that responded with  $\text{Ca}^{2+}$  increase on application of 50 mM KCl but not on low  $[\text{K}^+]$  were used in the subsequent analysis.

#### 5.10 Biotinylation assay

Rat cortical cultures (100,000 cells/cm<sup>2</sup>) were grown under standard conditions in 6-well plates as described above. DIV12 cultures were used for biotinylation assays. Pierce Cell Surface Protein Isolation Kit was used according to manufacturer's instructions with some modifications. In brief, cultures were placed on ice, rinsed twice in ice-cold PBS-Ca-Mg (PBS + 0.1 mM  $\text{CaCl}_2$  + 1 mM  $\text{MgCl}_2$ ) and then pre-incubated in 1.5 ml of cold PBS-Ca-Mg for 30 min at 4 °C. Cells were incubated in 1.5 ml of freshly prepared 0.25 mg/ml Sulfo-NHC-LC-Biotin diluted in cold PBS-Ca-Mg for 30 min at 4 °C. Cells were rinsed twice in cold PBS-Ca-Mg, and then a cold quenching solution containing 0.1 M glycine in PBS-Ca-Mg was added for 20 min. Cells were rinsed twice in cold PBS-Ca-Mg and collected by scraping into 250  $\mu$ l per well of lysis buffer containing protease inhibitors. Cell lysates were incubated for 15 min on ice, mixed, centrifuged at 10,000xg for 10 min at 4 °C, and supernatant was collected. Ten percent of the collected lysate was taken and stored for subsequent immunoblotting as a total protein sample. NeutrAvidin Agarose slurry (100  $\mu$ l) was loaded into Pierce columns and washed according to instructions. The clarified cell lysate (the remaining 90 %) was added to the agarose slurry and incubated overnight at +4 °C with rotation. The next day the column was centrifuged and the agarose beads were washed two times with 500  $\mu$ l of TNE buffer (1 % Nonidet P-40, 50 mM Tris-HCl, pH 8.0, 140 mM NaCl, 5 mM EDTA) supplemented with the Complete Protease Inhibitor Cocktail and the PhosStop phosphatase inhibitor cocktail (both from Roche Diagnostics, Mannheim, Germany), and then three times with 100  $\mu$ l of the Wash buffer (Pierce) with protease inhibitors. Proteins were eluted in 100  $\mu$ l of the SDS-PAGE sample buffer (62.5 mM Tris-HCl, pH 6.8, 1 % SDS, 10 % glycerol) containing 50 mM DTT. Samples were incubated for 60 min at room temperature with rotation, centrifuged for 2 min, and the eluate was collected. A trace amount of bromophenol blue was added and the samples were analyzed by immunoblotting as described above.

#### 5.11 Immunohistochemistry

Adult C57Bl/6JHsd (Harlan, Blackthorn Bicester, UK) mice of both sexes were used for immunohistochemistry. Mice were deeply anesthetized by pentobarbital and perfused with 4 % PFA in PBS. Brains were collected and postfixed in PFA for 2 h, cryoprotected in 30 % sucrose overnight, and frozen in TissueTek (O.C.T compound, Sakura). Free-floating cryosections (40  $\mu$ m) were used immediately for immunostaining or stored at -20 °C in a cryoprotective medium. Immunostainings were performed as described previously (Markkanen et al., 2014). To reduce the nonspecific signal, the KCC2a antiserum was preabsorbed against PFA-fixed tissue from KCC2a-KO mice, as described previously (Markkanen et al., 2014). P7 wild-type and KCC2b-deficient mice (Woo et al., 2002) were perfused with 4 % PFA in PBS, brains were collected and postfixed with the same fixative for 2h. Brains were soaked in 30 % sucrose in PBS for at least 24 h, and frozen in TissueTek. Coronal cryosections (20  $\mu$ m) were cut and placed on Superfrost Plus slides (Menzel-Gläser, Braunschweig, Germany), and stored at -20 °C until use. Sections were rinsed in PBS 3 times for 10 min and blocked with 5 % normal donkey serum and 0.3 % Triton X-100 in PBS for 30 min at room temperature. Sections were incubated with dilutions of primary antibody: rabbit anti-KCC2a antibody (1:750) or rabbit

anti-KCC2pan antibody (1:1,000) in a blocking buffer overnight at 4 °C. Sections were washed with PBS, incubated with donkey anti-rabbit IgG-Cy3 (1:150, Jackson) in a blocking buffer for 2h, washed with PBS, and finally mounted on slides with PBS-glycerol.

#### 5.12 Coimmunoprecipitation (coIP) assay

CoIP experiments were performed according to (Cai et al., 2002) with small modifications. Human embryonic kidney (HEK) 293 cells (CLR-1573, American Type Culture Collection, Manassas, VA) were cultured (in 10 cm plates) in DMEM supplemented with 10 % fetal bovine serum, 100 U/ml penicillin, 100 µg/ml streptomycin, and 2 mM L-glutamine. Cells were transfected with appropriate expression constructs using jetPEI cationic polymer transfection reagent (Polyplus-transfection Inc., NY) according to the manufacturer's protocol. Transfected HEK293 cells were rinsed twice with ice-cold PBS, lysed for 15 min in ice-cold TNE buffer (140 mM NaCl, 5 mM EDTA, 1 % Nonidet P-40, 50 mM Tris-HCl pH 8.0), supplemented with the Complete Protease Inhibitor Cocktail and the PhosStop phosphatase inhibitor cocktail (both from Roche Diagnostics, Mannheim, Germany), and centrifuged for 10 min at +4 °C to remove particulate matter. Supernatant was precleared for 1 h at +4 °C using blocked GammaBind G Sepharose (GE Healthcare, Uppsala, Sweden) and further incubated overnight with 2 µg of the appropriate antibody. Thereafter, the blocked protein-G Sepharose was added and incubation was continued for 2 h. After washing of the Sepharose beads twice with the ice-cold TNE buffer for 10 min and twice with PBS for 5 min, the bound proteins were eluted by SDS sample buffer (1 % SDS, 100 mM DTT, 50 mM Tris, pH 7.5) and separated by SDS-PAGE.

#### 5.13 Functional <sup>86</sup>Rb flux assay

Flux experiments were performed in HEK293 cells at room temperature as described previously (Uvarov et al., 2007) with small modifications. One day before the measurements, the cells were transfected with the indicated expression constructs using jetPEI cationic polymer transfection reagent (Polyplus-transfection Inc., NY, USA) according to the manufacturer's protocol. On the day of the flux experiments, the cells were washed three times in control medium (135 mM NaCl, 5 mM RbCl, 1 mM MgCl<sub>2</sub>, 1 mM CaCl<sub>2</sub>, 1 mM Na<sub>2</sub>HPO<sub>4</sub>, 2 mM Na<sub>2</sub>SO<sub>4</sub>, 3 mM glucose, 15 mM HEPES, pH 7.4, 0.1 mM ouabain, and 10 µM bumetanide) complemented when required with 2 mM furosemide. The cells were then incubated for 3 min in the control medium containing 2 µCi/ml <sup>86</sup>RbCl (PerkinElmer, MA). <sup>86</sup>Rb influx was terminated by five washings in ice-cold control medium containing 2 mM furosemide. Cells were dried and intensity of <sup>86</sup>Rb signal was analyzed using PhosphoImager (Fuji) by pre-exposing the culture plates with the phosphorimaging BAS-MP 2040S screen from Fuji (Tokyo, Japan).

#### 5.14 Statistical analysis

GraphPad Prism 5 (GraphPad Software, Inc, CA) was used to perform all statistical analysis including confirmation of similar variance between all groups compared and the Kolmogorov-Smirnov test for data normality. Significance was determined by the one-sample t-test when samples were compared to normalized control, by two-tailed unpaired Student's t-test when two groups were compared, or by one-way ANOVA with Bonferroni multiple comparisons test when more than two groups were compared. P-values less than 0.05 were considered significant.

#### Conflict of Interest Statement

The authors declare that the research was conducted in the absence of any commercial or financial relationships that could be construed as a potential conflict of interest.

**Acknowledgements:** We thank Kaija Berg for technical assistance, Seija Lågas and Outi Nikkilä for the neuronal cultures, Biff Forbush for the HA-SPAK and DNSPAK expression constructs, Hiroshi Ushiro for the anti-SPAK antibody, and the Biomedicum Imaging Unit for help with confocal microscopy and imaging. Supported by grants from the Academy of Finland (to AL, LK, CR, MSA & PU).

#### Authors and Contributors

MM, CR, MSA, and PU conceived the study. MM, AL, SK, EP, SS, LK, ED, CR, MSA, and PU designed the experiments. MM, AL, SK, EP, SS, ED and PU performed experiments. MM, AL, SK, EP, SS, LK, ED, CR, MSA, and PU analyzed the data and drafted the manuscript. MM, MSA, and PU wrote the manuscript.

#### References

- Acton BA, Mahadevan V, Mercado A, Uvarov P, Ding Y, Pressey J, Airaksinen MS, Mount DB, Woodin MA. 2012. Hyperpolarizing GABAergic transmission requires the KCC2 C-terminal ISO domain. *J. Neurosci.* **32**: 8746-8751.
- Alessi DR, Zhang J, Khanna A, Hochdorfer T, Shang Y, Kahle KT. 2014. The WNK-SPAK/OSR1 pathway: master regulator of cation-chloride cotransporters. *Sci. Signal.* **7**: re3.
- Antrobus SP, Lytle C, Payne JA. 2012. K<sup>+</sup>-Cl<sup>-</sup> cotransporter-2 KCC2 in chicken cardiomyocytes. *Am. J. Physiol. Cell. Physiol.* **303**: C1180-91.
- Austin TM, Nannemann DP, Deluca SL, Meiler J, Delpire E. 2014. In silico analysis and experimental verification of OSR1 kinase - Peptide interaction. *J. Struct. Biol.* **187**: 58-65.
- Banker G, Goslin K. 1998. *Culturing Nerve Cells* MIT Press: Cambridge, England. .
- Bartschat DK, Blaustein MP. 1985. Calcium-activated potassium channels in isolated presynaptic nerve terminals from rat brain. *J. Physiol.* **361**: 441-457.
- Blaesse P, Guillemin I, Schindler J, Schweizer M, Delpire E, Khiroug L, Friauf E, Nothwang HG. 2006. Oligomerization of KCC2 correlates with development of inhibitory neurotransmission. *J. Neurosci.* **26**: 10407-10419.
- Cai C, Coleman SK, Niemi K, Keinänen K. 2002. Selective binding of synapse-associated protein 97 to GluR-A alpha-amino-5-hydroxy-3-methyl-4-isoxazole propionate receptor subunit is determined by a novel sequence motif 5. *J. Biol. Chem.* **277**: 31484-31490.
- Casula S, Shmukler BE, Wilhelm S, Stuart-Tilley AK, Su W, Chernova MN, Brugnara C, Alper SL. 2001. A dominant negative mutant of the KCC1 K-Cl cotransporter: both N- and C-terminal cytoplasmic domains are required for K-Cl cotransport activity. *J. Biol. Chem.* **276**: 41870-41878.
- Chudotvorova I, Ivanov A, Rama S, Hubner CA, Pellegrino C, Ben Ari Y, Medina I. 2005. Early expression of KCC2 in rat hippocampal cultures augments expression of functional GABA synapses. *J. Physiol.* **566**: 671-679.

- Dallwig R, Deitmer JW. 2002. Cell-type specific calcium responses in acute rat hippocampal slices. *J. Neurosci. Methods* **116**: 77-87.
- Dallwig R, Vitten H, Deitmer JW. 2000. A novel barium-sensitive calcium influx into rat astrocytes at low external potassium. *Cell Calcium* **28**: 247-259.
- de Los Heros P, Alessi DR, Gourlay R, Campbell DG, Deak M, Macartney TJ, Kahle KT, Zhang J. 2014. The WNK-regulated SPAK/OSR1 kinases directly phosphorylate and inhibit the K<sup>+</sup>-Cl<sup>-</sup> co-transporters. *Biochem. J.* **458**: 559-573.
- Delpire E, Gagnon KB. 2008. SPAK and OSR1: STE20 kinases involved in the regulation of ion homeostasis and volume control in mammalian cells. *Biochem. J.* **409**: 321-331.
- Dowd BFX, Forbush B. 2003. PASK (proline-alanine-rich STE20-related kinase), a regulatory kinase of the Na-K-Cl cotransporter (NKCC1) 1. *J. Biol. Chem.* **278**: 27347-27353.
- Filippi BM, de los Heros P, Mehellou Y, Navratilova I, Gourlay R, Deak M, Plater L, Toth R, Zeqiraj E, Alessi DR. 2011. MO25 is a master regulator of SPAK/OSR1 and MST3/MST4/YSK1 protein kinases. *EMBO J.* **30**: 1730-1741.
- Fiumelli H, Cancedda L, Poo MM. 2005. Modulation of GABAergic transmission by activity via postsynaptic Ca<sup>2+</sup>-dependent regulation of KCC2 function. *Neuron* **48**: 773-786.
- Fiumelli H, Briner A, Puskarjov M, Blaesse P, Belem BJ, Dayer AG, Kaila K, Martin JL, Vutskits L. 2013. An ion transport-independent role for the cation-chloride cotransporter KCC2 in dendritic spinogenesis in vivo. *Cereb. Cortex* **23**: 378-388.
- Friedel P, Kahle KT, Zhang J, Hertz N, Pisella LI, Buhler E, Schaller F, Duan J, Khanna AR, Bishop PN, Shokat KM, Medina I. 2015. WNK1-regulated inhibitory phosphorylation of the KCC2 cotransporter maintains the depolarizing action of GABA in immature neurons. *Sci. Signal.* **8**: ra65.
- Fujii T, Takahashi Y, Itomi Y, Fujita K, Morii M, Tabuchi Y, Asano S, Tsukada K, Takeguchi N, Sakai H. 2008. K<sup>+</sup>-Cl<sup>-</sup> Cotransporter-3a Up-regulates Na<sup>+</sup>,K<sup>+</sup>-ATPase in Lipid Rafts of Gastric Luminal Parietal Cells. *J. Biol. Chem.* **283**: 6869-6877.
- Gagnon KB, England R, Delpire E. 2006a. Characterization of SPAK and OSR1, regulatory kinases of the Na-K-2Cl cotransporter. *Mol. Cell. Biol.* **26**: 689-698.
- Gagnon KB, England R, Delpire E. 2006b. Volume sensitivity of cation-Cl<sup>-</sup> cotransporters is modulated by the interaction of two kinases: Ste20-related proline-alanine-rich kinase and WNK4. *Am. J. Physiol Cell Physiol.* **290**: C134-C142.
- Geng Y, Hoke A, Delpire E. 2009. The Ste20 Kinases Ste20-related Proline-Alanine-rich Kinase and Oxidative-stress Response 1 Regulate NKCC1 Function in Sensory Neurons. *J. Biol. Chem.* **284**: 14020-14028.
- Grynkiewicz G, Poenie M, Tsien RY. 1985. A new generation of Ca<sup>2+</sup> indicators with greatly improved fluorescence properties. *J. Biol. Chem.* **260**: 3440-3450.

Hartmann AM, Blaesse P, Kranz T, Wenz M, Schindler J, Kaila K, Friauf E, Nothwang HG. 2009. Opposite effect of membrane raft perturbation on transport activity of KCC2 and NKCC1. *J. Neurochem.* **111**: 321-331.

Hekmat-Safe DS, Lundy MY, Ranga R, Tanouye MA. 2006. Mutations in the K<sup>+</sup>/Cl<sup>-</sup> cotransporter gene *kazachoc* (*kcc*) increase seizure susceptibility in *Drosophila*. *J. Neurosci.* **26**: 8943-8954.

Horn Z, Ringstedt T, Blaesse P, Kaila K, Herlenius E. 2010. Premature expression of KCC2 in embryonic mice perturbs neural development by an ion transport-independent mechanism. *Eur. J. Neurosci.* **31**: 2142-2155.

Hubner CA, Stein V, Hermans-Borgmeyer I, Meyer T, Ballanyi K, Jentsch TJ. 2001. Disruption of KCC2 reveals an essential role of K-Cl cotransport already in early synaptic inhibition. *Neuron* **30**: 515-524.

Ikeda K, Onimaru H, Yamada J, Inoue K, Ueno S, Onaka T, Toyoda H, Arata A, Ishikawa TO, Taketo MM, Fukuda A, Kawakami K. 2004. Malfunction of respiratory-related neuronal activity in Na<sup>+</sup>, K<sup>+</sup>-ATPase alpha2 subunit-deficient mice is attributable to abnormal Cl<sup>-</sup> homeostasis in brainstem neurons. *J. Neurosci.* **24**: 10693-10701.

Inoue K, Furukawa T, Kumada T, Yamada J, Wang T, Inoue R, Fukuda A. 2012. Taurine inhibits K<sup>+</sup>-Cl<sup>-</sup> cotransporter KCC2 to regulate embryonic Cl<sup>-</sup> homeostasis via with-no-lysine (Wnk) protein kinase signaling pathway. *J. Biol. Chem.* **287**: 20839-20850.

Johnston AM, Naselli G, Gonez LJ, Martin RM, Harrison LC, DeAizpurua HJ. 2000. SPAK, a STE20/SPS1-related kinase that activates the p38 pathway. *Oncogene* **19**: 4290-4297.

Kahle KT, Delpire E. 2016. Kinase-KCC2 coupling: Cl<sup>-</sup> rheostasis, disease susceptibility, therapeutic target. *J. Neurophysiol.* **115**: 8-18.

Kahle KT, Merner ND, Friedel P, Silayeva L, Liang B, Khanna A, Shang Y, Lachance-Touchette P, Bourassa C, Levert A, Dion PA, Walcott B, Spiegelman D, Dionne-Laporte A, Hodgkinson A, Awadalla P, Nikbakht H, Majewski J, Cossette P, Deeb TZ, Moss SJ, Medina I, Rouleau GA. 2014. Genetically encoded impairment of neuronal KCC2 cotransporter function in human idiopathic generalized epilepsy. *EMBO Rep.* **15**: 766-774.

Kaila K, Price TJ, Payne JA, Puskarjov M, Voipio J. 2014. Cation-chloride cotransporters in neuronal development, plasticity and disease. *Nat. Rev. Neurosci.* **15**: 637-654.

Khirug S, Huttu K, Ludwig A, Smirnov S, Voipio J, Rivera C, Kaila K, Khiroug L. 2005. Distinct properties of functional KCC2 expression in immature mouse hippocampal neurons in culture and in acute slices. *Eur. J. Neurosci.* **21**: 899-904.

Lee H, Chen CX, Liu YJ, Aizenman E, Kandler K. 2005. KCC2 expression in immature rat cortical neurons is sufficient to switch the polarity of GABA responses. *Eur. J. Neurosci.* **21**: 2593-2599.

Lee SJ, Cobb MH, Goldsmith EJ. 2009. Crystal structure of domain-swapped STE20 OSR1 kinase domain. *Protein Sci.* **18**: 304-313.

Leinekugel X, Tseeb V, Ben Ari Y, Bregestovski P. 1995. Synaptic GABAA activation induces  $Ca^{2+}$  rise in pyramidal cells and interneurons from rat neonatal hippocampal slices. *J. Physiol.* **487**: 319-329.

Leonzino M, Busnelli M, Antonucci F, Verderio C, Mazzanti M, Chini B. 2016. The Timing of the Excitatory-to-Inhibitory GABA Switch Is Regulated by the Oxytocin Receptor via KCC2. *Cell. Rep.* **15**: 96-103.

Li H, Khirug S, Cai C, Ludwig A, Blaesse P, Kolikova J, Afzalov R, Coleman SK, Lauri S, Airaksinen MS, Keinänen K, Khiroug L, Saarma M, Kaila K, Rivera C. 2007. KCC2 interacts with the dendritic cytoskeleton to promote spine development. *Neuron* **56**: 1019-1033.

Liu ZP, Neff RA, Berg DK. 2006. Sequential interplay of nicotinic and GABAergic signaling guides neuronal development. *Science* **314**: 1610-1613.

Llano O, Smirnov S, Soni S, Golubtsov A, Guillemin I, Hotulainen P, Medina I, Nothwang HG, Rivera C, Ludwig A. 2015. KCC2 regulates actin dynamics in dendritic spines via interaction with beta-PIX. *J. Cell Biol.* **209**: 671-686.

Ludwig A, Li H, Saarma M, Kaila K, Rivera C. 2003. Developmental up-regulation of KCC2 in the absence of GABAergic and glutamatergic transmission. *Eur. J. Neurosci.* **18**: 3199-3206.

Mahadevan V, Pressey JC, Acton BA, Uvarov P, Huang MY, Chevrier J, Puchalski A, Li CM, Ivakine EA, Airaksinen MS, Delpire E, McInnes RR, Woodin MA. 2014. Kainate receptors coexist in a functional complex with KCC2 and regulate chloride homeostasis in hippocampal neurons. *Cell. Rep.* **7**: 1762-1770.

Markkanen M, Karhunen T, Llano O, Ludwig A, Rivera C, Uvarov P, Airaksinen MS. 2014. Distribution of neuronal KCC2a and KCC2b isoforms in mouse CNS. *J. Comp. Neurol.* **522**: 1897-1914.

Mercado A, Broumand V, Zandi-Nejad K, Enck AH, Mount DB. 2006. A C-terminal domain in KCC2 confers constitutive  $K^{+}$ - $Cl^{-}$  cotransport. *J. Biol. Chem.* **281**: 1016-1026.

Payne JA. 1997. Functional characterization of the neuronal-specific K-Cl cotransporter: implications for  $[K^{+}]_o$  regulation. *Am. J. Physiol.* **273**: C1516-C1525.

Payne JA, Stevenson TJ, Donaldson LF. 1996. Molecular characterization of a putative K-Cl cotransporter in rat brain. A neuronal-specific isoform. *J. Biol. Chem.* **271**: 16245-16252.

Piechotta K, Garbarini N, England R, Delpire E. 2003. Characterization of the interaction of the stress kinase SPAK with the  $Na^{+}$ - $K^{+}$ - $2Cl^{-}$  cotransporter in the nervous system: evidence for a scaffolding role of the kinase. *J. Biol. Chem.* **278**: 52848-52856.

Puskarjov M, Seja P, Heron SE, Williams TC, Ahmad F, Iona X, Oliver KL, Grinton BE, Vutskits L, Scheffer IE, Petrou S, Blaesse P, Dibbens LM, Berkovic SF, Kaila K. 2014. A variant of KCC2 from patients with febrile seizures impairs neuronal  $Cl^{-}$  extrusion and dendritic spine formation. *EMBO Rep.* **15**: 723-729.

Richardson C, Rafiqi FH, Karlsson HK, Moleleki N, Vandewalle A, Campbell DG, Morrice NA, Alessi DR. 2008. Activation of the thiazide-sensitive Na<sup>+</sup>-Cl<sup>-</sup> cotransporter by the WNK-regulated kinases SPAK and OSR1. *J. Cell. Sci.* **121**: 675-684.

Rinehart J, Maksimova YD, Tanis JE, Stone KL, Hodson CA, Zhang J, Risinger M, Pan W, Wu D, Colangelo CM, Forbush B, Joiner CH, Gulcicek EE, Gallagher PG, Lifton RP. 2009. Sites of regulated phosphorylation that control K-Cl cotransporter activity. *Cell* **138**: 525-536.

Rivera C, Voipio J, Payne JA, Ruusuvuori E, Lahtinen H, Lamsa K, Pirvola U, Saarma M, Kaila K. 1999. The K<sup>+</sup>/Cl<sup>-</sup> co-transporter KCC2 renders GABA hyperpolarizing during neuronal maturation. *Nature* **397**: 251-255.

Saito H, Watanabe M, Akita T, Ohba C, Sugai K, Ong WP, Shiraishi H, Yuasa S, Matsumoto H, Beng KT, Saitoh S, Miyatake S, Nakashima M, Miyake N, Kato M, Fukuda A, Matsumoto N. 2016. Impaired neuronal KCC2 function by biallelic SLC12A5 mutations in migrating focal seizures and severe developmental delay. *Sci. Rep.* **6**: 30072.

Shen MR, Chou CY, Hsu KF, Hsu YM, Chiu WT, Tang MJ, Alper SL, Ellory JC. 2003. KCl cotransport is an important modulator of human cervical cancer growth and invasion. *J. Biol. Chem.* **278**: 39941-39950.

Simard CF, Bergeron MJ, Frenette-Cotton R, Carpentier GA, Pelchat ME, Caron L, Isenring P. 2007. Homooligomeric and heterooligomeric associations between K<sup>+</sup>-Cl<sup>-</sup> cotransporter isoforms and between K<sup>+</sup>-Cl<sup>-</sup> and Na<sup>+</sup>-K<sup>+</sup>-Cl<sup>-</sup> cotransporters. *J. Biol. Chem.* **282**: 18083-18093.

Sokka AL, Putkonen N, Mudo G, Pryazhnikov E, Reijonen S, Khiroug L, Belluardo N, Lindholm D, Korhonen L. 2007. Endoplasmic reticulum stress inhibition protects against excitotoxic neuronal injury in the rat brain. *J. Neurosci.* **27**: 901-908.

Stil A, Jean-Xavier C, Liabeuf S, Brocard C, Delpire E, Vinay L, Viemari JC. 2011. Contribution of the potassium-chloride co-transporter KCC2 to the modulation of lumbar spinal networks in mice. *Eur. J. Neurosci.* **33**: 1212-1222.

Stodberg T, McTague A, Ruiz AJ, Hirata H, Zhen J, Long P, Farabella I, Meyer E, Kawahara A, Vassallo G, Stivaros SM, Bjursell MK, Stranneheim H, Tigerschiold S, Persson B, Bangash I, Das K, Hughes D, Lesko N, Lundeberg J, Scott RC, Poduri A, Scheffer IE, Smith H, Gissen P, Schorge S, Reith ME, Topf M, Kullmann DM, Harvey RJ, Wedell A, Kurian MA. 2015. Mutations in SLC12A5 in epilepsy of infancy with migrating focal seizures. *Nat. Commun.* **6**: 8038.

Tanis JE, Bellemer A, Moresco JJ, Forbush B, Koelle MR. 2009. The potassium chloride cotransporter KCC-2 coordinates development of inhibitory neurotransmission and synapse structure in *Caenorhabditis elegans*. *J. Neurosci.* **29**: 9943-9954.

Tao R, Li C, Newburn EN, Ye T, Lipska BK, Herman MM, Weinberger DR, Kleinman JE, Hyde TM. 2012. Transcript-specific associations of SLC12A5 (KCC2) in human prefrontal cortex with development, schizophrenia, and affective disorders. *J. Neurosci.* **32**: 5216-5222.

- Taylor CA, 4th, Juang YC, Earnest S, Sengupta S, Goldsmith EJ, Cobb MH. 2015. Domain-Swapping Switch Point in Ste20 Protein Kinase SPAK. *Biochemistry* **54**: 5063-5071.
- Titz S, Sammler EM, Hormuzdi SG. 2015. Could tuning of the inhibitory tone involve graded changes in neuronal chloride transport? *Neuropharmacology* **95**: 321-331.
- Tornberg J, Voikar V, Savilahti H, Rauvala H, Airaksinen MS. 2005. Behavioural phenotypes of hypomorphic KCC2-deficient mice. *Eur. J. Neurosci.* **21**: 1327-1337.
- Tsutsumi T, Ushiro H, Kosaka T, Kayahara T, Nakano K. 2000. Proline- and alanine-rich Ste20-related kinase associates with F-actin and translocates from the cytosol to cytoskeleton upon cellular stresses. *J. Biol. Chem.* **275**: 9157-9162.
- Ushiro H, Tsutsumi T, Suzuki K, Kayahara T, Nakano K. 1998. Molecular cloning and characterization of a novel Ste20-related protein kinase enriched in neurons and transporting epithelia 1. *Arch. Biochem. Biophys.* **355**: 233-240.
- Uvarov P. 2010. Neuronal K-Cl Cotransporter: Transcriptional Mechanisms of KCC2 Gene Regulation. [dissertation]. [Helsinki]: Helsinki University Press. Available online at: <https://helda.helsinki.fi/handle/10138/22378>. .
- Uvarov P, Ludwig A, Markkanen M, Rivera C, Airaksinen MS. 2006. Upregulation of the neuron-specific K<sup>+</sup>/Cl<sup>-</sup> cotransporter expression by transcription factor early growth response 4. *J. Neurosci.* **26**: 13463-13473.
- Uvarov P, Ludwig A, Markkanen M, Soni S, Hubner CA, Rivera C, Airaksinen MS. 2009. Coexpression and heteromerization of two neuronal K-Cl cotransporter isoforms in neonatal brain. *J. Biol. Chem.* **284**: 13696-13704.
- Uvarov P, Ludwig A, Markkanen M, Pruunsild P, Kaila K, Delpire E, Timmusk T, Rivera C, Airaksinen MS. 2007. A novel N-terminal isoform of the neuron-specific K-Cl cotransporter KCC2. *J. Biol. Chem.* **282**: 30570-30576.
- Villa F, Goebel J, Rafiqi FH, Deak M, Thastrup J, Alessi DR, van Aalten DM. 2007. Structural insights into the recognition of substrates and activators by the OSR1 kinase. *EMBO Rep.* **8**: 839-845.
- Vitari AC, Thastrup J, Rafiqi FH, Deak M, Morrice NA, Karlsson HK, Alessi DR. 2006. Functional interactions of the SPAK/OSR1 kinases with their upstream activator WNK1 and downstream substrate NKCC1. *Biochem. J.* **397**: 223-231.
- Watanabe M, Wake H, Moorhouse AJ, Nabekura J. 2009. Clustering of neuronal K<sup>+</sup>-Cl<sup>-</sup> cotransporters in lipid rafts by tyrosine phosphorylation. *J. Biol. Chem.* **284**: 27980-27988.
- Williams JR, Sharp JW, Kumari VG, Wilson M, Payne JA. 1999. The neuron-specific K-Cl cotransporter, KCC2. Antibody development and initial characterization of the protein. *J. Biol. Chem.* **274**: 12656-12664.

Woo NS, Lu J, England R, McClellan R, Dufour S, Mount DB, Deutch AY, Lovinger DM, Delpire E. 2002. Hyperexcitability and epilepsy associated with disruption of the mouse neuronal-specific K-Cl cotransporter gene. *Hippocampus* **12**: 258-268.

Xu JC, Lytle C, Zhu TT, Payne JA, Benz E, Jr, Forbush B, III. 1994. Molecular cloning and functional expression of the bumetanide-sensitive Na-K-Cl cotransporter. *Proc. Natl. Acad. Sci. U. S. A.* **91**: 2201-2205.

Zhu L, Lovinger D, Delpire E. 2005. Cortical neurons lacking KCC2 expression show impaired regulation of intracellular chloride. *J. Neurophysiol.* **93**: 1557-1568.

## [Figure legends]

### Figure 1.

#### Proportion of KCC2a to the total KCC2 protein and mRNA expression in maturing dissociated cortical cultures

A) Western blot analysis of KCC2a, KCC2pan (KCC2a+KCC2b), and SPAK proteins in rat cortical cultures at different time points. Neuronal marker  $\beta$ -tubulin was used as a loading control to normalize the expression data. Note that due to limited lower total protein content only 10  $\mu$ g was loaded for DIV2 samples.

B) Quantification of the Western blot data obtained from three independent cultures; shown are means (solid circles) and individual values (empty circles). Total KCC2 (KCC2a+KCC2b) levels grow more rapidly compared to the KCC2a protein levels during the first two weeks in culture. The developmental expression profiles for KCC2a and total KCC2 proteins were normalized to the total KCC2 level at DIV2. At DIV14, ~80 % of total KCC2 protein corresponds to KCC2b and ~20 % to KCC2a. Data are mean  $\pm$  SEM. (\*,  $p < 0.05$ ; \*\*\*,  $p < 0.001$ ; ns, not significant, Student's t-test,  $n = 3$ ). SPAK expression is upregulated robustly during the first week in culture, but is stabilized during second week. Values are mean  $\pm$  SEM. (\*,  $p < 0.05$ ; ns, not significant, Student's t-test,  $n = 3$ ).

C) Quantitative real-time PCR analysis of KCC2a and KCC2 total mRNA expression relative to GAPDH in DIV2, DIV8 and DIV14 dissociated cortical cultures. The developmental mRNA expression profiles for KCC2a and KCC2 total were normalized to GAPDH and plotted relative to the total KCC2 expression at DIV2. Means (solid circles) and individual values (empty circles) are shown. Data are mean  $\pm$  SEM. (\*,  $p < 0.05$ ; \*\*\*,  $p < 0.001$ ; ns, not significant, Student's t-test,  $n = 4$ ).

### Figure 2.

#### KCC2a is functional in transfected cultured hippocampal neurons

The efficacy of K-Cl cotransport mediated by KCC2a was determined by estimating its capacity to induce a somatodendritic chloride gradient in DIV10 neurons from KCC2-null mutant mice co-transfected at DIV8 with KCC2a (and EGFP) or control (EGFP only) expression vector.

A) Schematic depiction of the method, which includes whole-cell patch-clamp recordings under a constant Cl<sup>-</sup> load via a somatic patch pipette. KCC2 molecules are depicted by gray circles at the surface of the soma and dendrite. Recordings were done always from soma, but GABA uncaging (by UV-mediated focal photolysis) was done for each neuron consequently at the soma and at a proximal dendritic location.

B) Shown is a wide-field image of immunostaining with KCC2pan antibody of a KCC2a-transfected neuron expressing KCC2a in the soma and dendrites. Two insets on the right are overexposed from the same image (marked by rectangles) and allow comparing levels of immunoreactivity produced by the KCC2pan antibody in the KCC2a-transfected neuron and in the neighbor non-transfected KCC2-KO neuron (marked by the asterisk). Scale bar is 20  $\mu\text{m}$ .

C) Whole-cell patch-clamp recordings under a constant  $\text{Cl}^-$  load via a somatic patch pipette were used to assess an imposed  $E_{\text{GABA}}$  somatodendritic gradient. Recordings were performed always from soma, but GABA uncaging (marked by line above the traces) was done separately at the soma and at the proximal dendritic location. Shown are typical traces and I-V plots of the  $\text{GABA}_A$  responses of uncaging at the soma ( $\blacksquare$ , bottom right traces) and at the dendrite ( $\square$ , top left traces) of a neuron transfected with KCC2a (left panel) and a control neuron transfected with EGFP only (right panel). I-V curves were plotted based on the specimen recordings shown in the insets, and were normalized with respect to peak  $I_{\text{GABA}}$  at the most negative holding potential ( $V_h$ ) tested in the experiment.

D) The histogram shows the imposed somatodendritic gradient of  $E_{\text{GABA}}$  in the hippocampal neurons (from KCC2-null mutant mice) transfected with KCC2a or control vector. Values are mean  $\pm$  SEM. (\*\*,  $p < 0.01$ , Student's t-test; number of analyzed neurons is indicated under the corresponding bars).

### Figure 3.

#### **KCC2a overexpression attenuates depolarizing $\text{GABA}_A$ responses in cultured neurons**

A) Four images for a typical Fura-2 AM calcium imaging protocol are shown: bright field image of a whole optical field (upper left); the same optical field obtained with GFP-filter for identification of transfected cells (upper right); Fura-340 signal, which was weak due to usage of suboptimum 10x objective lens (lower left), and Fura-380 signal, which was used for subsequent analysis (lower right). Regions of interest (ROIs) chosen for cell soma regions are shown for the GFP-positive cells (yellow circles, ROI1-ROI7). Scale bar is 100  $\mu\text{m}$ .

B) Muscimol induces  $\text{Ca}^{2+}$  increase in the cortical neurons. To discriminate between glial cells and neurons, we used a previously described protocol that takes into account their different  $\text{Ca}^{2+}$  responses on application of low external  $[\text{K}^+]$  (Dallwig and Deitmer, 2002). Exogenous KCC2a and KCC2b prevent the  $\text{Ca}^{2+}$  increase induced by muscimol. Shown are representative responses of individual cells from different transfections.

C) Quantification of the calcium responses in DIV6 cortical cultures shows that overexpression of KCC2a and KCC2b attenuates the muscimol-elicited depolarizing GABA responses. Number of independent experiments (plates) analyzed is indicated. The number of cells measured in each plate was 20 to 40. Values are means ( $\pm$  SEM) of percentile (% of responding cells in each plate). (\*\*\*,  $p < 0.001$ , ANOVA, Bonferroni multiple comparisons test, ns = not significant).

### Figure 4.

#### **Subcellular localization of endogenous KCC2a and KCC2b in primary neuronal cultures**

A) Endogenous expression of KCC2 isoforms in methanol fixed dissociated cortical cultures derived from E18 rat embryos and cultured for two weeks *in vitro* (DIV14). Pseudocolor images of cortical neurons immunostained with antibodies against KCC2a or KCC2b are shown. Pseudocolors were designated as red (highest expression) to dark blue (lowest expression). KCC2b immunoreactivity is localized nearby the cell surface, but signal is also seen in intracellular compartments in the soma region as well as in dendrites. In parallel cultures immunostained with KCC2a antibodies, the immunoreactivity is mainly intracellular within soma and dendrites. The optical section images were acquired with a 63 $\times$  oil-immersion objective under a Zeiss LSM5 Pascal confocal microscope. Scale bar is 10  $\mu\text{m}$ .

B) Cell surface expression of KCC2 isoforms was studied in dissociated cortical cultures with a biotinylation assay. Cells were derived from E18 rat embryos and cultured for two weeks *in vitro* (DIV12). Surface-expressed proteins (and total protein) were detected by immunoblot analysis with antibodies to KCC2a, KCC2b and KCC2pan antibodies (and  $\beta$ -tubulin antibodies as a control).

C) Quantification of the biotinylated band intensities normalized to the total band intensities demonstrated that ~40 % of total endogenous KCC2a as well as KCC2b (monomers) are expressed on the surface. (n=3).

### Figure 5.

#### **KCC2a immunoreactivity is detected at the somatic surface in certain mouse brain areas**

A) In PFA-fixed wild-type adult mouse brain sections double-labeled with antibodies to KCC2a and KCC2b, KCC2a-labeling is seen only in the subiculum (marked with asterisk), whereas KCC2b staining is found throughout the hippocampal formation. The wide-field fluorescence images were obtained by using a 10 $\times$  objective under a Zeiss Axioplan 2 microscope and an AxioCam HR camera. Scale bar is 500  $\mu$ m.

B) Confocal images from subiculum (from the location marked with an asterisk in A), hypothalamus and medulla are shown. Somas (asterisks) and dendrites (arrows) are marked in the merged images. KCC2a signal (green) can be observed nearby the surface of somas and dendrites in subiculum and hypothalamus. However, in the medulla KCC2a is not visible nearby the soma surface, in contrast to KCC2b (red). In the putative dendritic profiles, KCC2a and KCC2b signals are not completely colocalized (yellow in merged images). The optical section images were acquired with a 40 $\times$  (NA 1.2) water-immersion objective under a Leica TCS SP8 confocal microscope. Scale bar is 20  $\mu$ m.

### Figure 6.

#### **SPAK reveals higher binding affinity to KCC2a than to KCC2b isoform**

A) Conservation of the putative SPAK binding site of KCC2a among CCC family members. The N-terminal part of KCC1 contains a similar amino acid sequence HFTV, which has been shown to bind OSR1 (Austin et al., 2014). KCC4a isoform containing SPAK/OSR1-binding motif has been predicted previously (Uvarov, 2010).

B) KCC2a or KCC2b expression vectors (or an empty vector) were co-expressed with an HA-tagged SPAK expression vector (HA-SPAK) in HEK293 cells. Forty-eight hours after the transfection, the cells were lysed and subjected to co-immunoprecipitation (coIP) with KCC2pan antibodies (IP: KCC2pan). Binding partners of the KCC2a and KCC2b proteins were analyzed by Western blot with the indicated antibodies (IB). The KCC2pan antibody efficiently precipitated both KCC2a and KCC2b proteins from the cell lysates (*upper panel* of the IP: KCC2pan part). The HA-SPAK protein was detected from cells co-expressing HA-SPAK and KCC2a, but not from cells co-expressing HA-SPAK and KCC2b (*lower panel* of the IP: KCC2pan part). The presence of KCC2a, KCC2b, and HA-SPAK proteins in the lysates was confirmed with the corresponding antibodies (Input).

C) CoIP with the anti-HA antibody (IP: HA) and detection with KCC2a confirm that KCC2a can interact with HA-SPAK (*middle panel* of the IP: HA part). Note that the KCC2 isoforms detected after coIP with HA were mostly of higher order associates (asterisk), possibly due to the KCC2 aggregation induced by heating (required for dissociation of the precipitated protein complexes from the beads). Expression of KCC2a, KCC2b, and HA-SPAK proteins in the cell lysates is also shown (Input).

### Figure 7.

#### **SPAK inhibits the furosemide-sensitive $^{86}$ Rb uptake mediated by KCC2a**

A) Immunocytochemistry with antibodies to KCC2pan in methanol-fixed HEK cells overexpressing KCC2a and KCC2b shows that both isoforms are located nearby the cell surface (red). Images are shown with blue DAPI stained nuclei (left) and without DAPI (right). The optical section images were acquired with a 63× oil-immersion objective under a Zeiss LSM5 Pascal confocal microscope. Scale bar is 10  $\mu\text{m}$ .

B) Furosemide-sensitive  $^{86}\text{Rb}$  uptake was measured in HEK293 cells transfected with KCC2a, KCC2b, or empty vector plasmids. Bumetanide (10  $\mu\text{M}$ ) and ouabain (100  $\mu\text{M}$ ) were added to prevent  $^{86}\text{Rb}$  flux through NKCC1 and Na/K-ATPase, respectively. Furosemide-sensitive  $^{86}\text{Rb}$  uptake was more than 30 times higher in cells expressing KCC2a or KCC2b than in cells transfected with an empty vector. Values are mean  $\pm$  SEM. (\*  $p < 0.05$ , ANOVA, Bonferroni multiple comparisons test,  $n=4$ ). Representative autoradiography images of the wells containing monolayers of HEK293 cells after the  $^{86}\text{Rb}$  uptake are shown below (see Methods).

C) Co-expression of KCC2a and SPAK (*left panel, grey bar*) resulted in significant downregulation of the furosemide-sensitive  $^{86}\text{Rb}$  uptake compared to cells cotransfected with KCC2a and empty vector (*left panel, open bar*) ( $81 \pm 6\%$ , \*  $p < 0.05$  compared with KCC2a control, one-sample t-test,  $n=6$ ). Co-expression of KCC2b with SPAK (*right panel, grey bar*) did not significantly change the furosemide-sensitive  $^{86}\text{Rb}$  uptake compared with KCC2b control (*right panel, open bar*) ( $109 \pm 9\%$ ,  $p > 0.05$ , one-sample t-test,  $n=6$ ). However, co-expression with DN-SPAK increased both KCC2a (*left panel, filled bar*) (\*,  $p < 0.05$  compared with KCC2a control, one-sample t-test,  $n=6$ ) and KCC2b-mediated  $^{86}\text{Rb}$  uptake (*right panel, filled bar*) (\*\*,  $p < 0.01$  compared with KCC2b control, one-sample t-test,  $n=6$ ).

KCC2a isoform is expressed at the neuronal plasma membrane  
KCC2a isoform mediates chloride extrusion in cultured neurons  
SPAK differently regulates kinetic activity of KCC2a and KCC2b isoforms

ACCEPTED MANUSCRIPT